

AFRL-VA-WP-TR-2000-3043

**DEVELOPMENT OF THE
AERODYNAMIC/AEROSERVOELASTIC
MODULES IN ASTROS**

**VOLUME IV - AEROSERVOELASTICITY DISCIPLINE IN
ASTROS, THEORETICAL MANUAL**

**ZONA TECHNOLOGY INC
7434 E STETSON DR SUITE 205
SCOTTSDALE AZ 85251**



FINAL REPORT FOR 9/1/96 -- 9/30/98

Approved for public release; distribution unlimited.

**Air Vehicles Directorate
Air Force Research Laboratory
Air Force Materiel Command
Wright-Patterson AFB, OH 45433-7542**

DTIC QUALITY INSPECTED 4

20001107 110

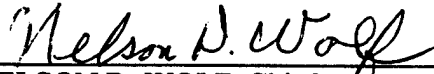
NOTICE

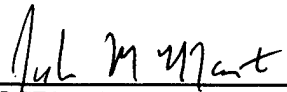
USING GOVERNMENT DRAWINGS, SPECIFICATIONS, OR OTHER DATA INCLUDED IN THIS DOCUMENT FOR ANY PURPOSE OTHER THAN GOVERNMENT PROCUREMENT DOES NOT IN ANY WAY OBLIGATE THE UNITED STATES GOVERNMENT. THE FACT THAT THE GOVERNMENT FORMULATED OR SUPPLIED THE DRAWINGS, SPECIFICATIONS, OR OTHER DATA DOES NOT LICENSE THE HOLDER OR ANY OTHER PERSON OR CORPORATION; OR CONVEY ANY RIGHTS OR PERMISSION TO MANUFACTURE, USE, OR SELL ANY PATENTED INVENTION THAT MAY BE RELATED TO THEM.

THIS REPORT IS RELEASEABLE TO THE NATIONAL TECHNICAL INFORMATION SERVICE (NTIS). AT NTIS, IT WILL BE AVAILABLE TO THE GENERAL PUBLIC, INCLUDING FOREIGN NATIONS.

THIS TECHNICAL REPORT HAS BEEN REVIEWED AND IS APPROVED FOR PUBLICATION.


VICTORIA A. TISCHLER
Aerospace Engineer
Structural Design & Development Branch


NELSON D. WOLF, Chief
Structural Design and Development Branch
Structures Division


JOSEPH M. MANTER, Chief
Structures Division
Air Vehicles Directorate

COPIES OF THIS REPORT SHOULD NOT BE RETURNED UNLESS RETURN IS REQUIRED BY SECURITY CONSIDERATIONS, CONTRACTUAL OBLIGATIONS, OR NOTICE ON A SPECIFIED DOCUMENT.

REPORT DOCUMENTATION PAGE			Form Approved OMB No. 0704-0188	
Public reporting burden for this collection of information is estimated to average 1 hour per response, including the time for reviewing instructions, searching existing data sources, gathering and maintaining the data needed, and completing and reviewing the collection of information. Send comments regarding this burden estimate or any other aspect of this collection of information, including suggestions for reducing this burden, to Washington Headquarters Services, Directorate for Information Operations and Reports, 1215 Jefferson Davis Highway, Suite 1204, Arlington, VA 22202-4302, and to the Office of Management and Budget, Paperwork Reduction Project (0704-0188), Washington, DC 20503.				
1. AGENCY USE ONLY (Leave blank)		2. REPORT DATE FEBRUARY 04, 1999	3. REPORT TYPE AND DATES COVERED FINAL 24 SEP 1996 - SEP 1998	
4. TITLE AND SUBTITLE DEVELOPMENT OF THE AERODYNAMIC/AEROSERVOELASTIC MODULES IN ASTROS / VOLUME IV - AEROSERVOELASTICITY DISCIPLINE IN ASTROS THEORETICAL MANUAL			5. FUNDING NUMBERS C: F33615-96-C-3217 PE: 65502F PR: STTR TA: 41 WU: 00	
6. AUTHOR(S) M. Karpel and B. Moulin Technion - I.I.T.				
7. PERFORMING ORGANIZATION NAME(S) AND ADDRESS(ES) Subcontractor to Research Insititute: Prime Contractor: Technion - Israel Institute of Technology ZONA Technology, Inc. Haifa 32000 7434 E. Stetson Drive, Suite 205 Israel Scottsdale, AZ 85251 Tel 972-4-8293490 / Fax 972-4-8229352 Tel (602) 945-9988 / Fax (602) 945-6588			8. PERFORMING ORGANIZATION REPORT NUMBER ZONA 99-11H	
9. SPONSORING/MONITORING AGENCY NAME(S) AND ADDRESS(ES) Air Vehicles Directorate Air Force Research Laboratory Air Force Materiel Command Wright Patterson Air Force Base OH 45433-7531 POC: Capt. Gerald Andersen. (937) 255-6992 / Dr. V.B.Venkavva (937) 255-2582			10. SPONSORING/MONITORING AGENCY REPORT NUMBER AFRL-VA-WP-TR-2000-3043	
11. SUPPLEMENTARY NOTES				
12a. DISTRIBUTION AVAILABILITY STATEMENT APPROVED FOR PUBLIC RELEASE; DISTRIBUTION UNLIMITED			12b. DISTRIBUTION CODE	
13. ABSTRACT (Maximum 200 words) This report presents the theoretical formulation of the aeroservoelastic module in ASTROS. Areas covered include the following: generalized matrices, rational aerodynamic approximations, state-space aeroservoelastic equations, flutter analysis, control stability margins and continuous gust response. This report is part of the documentation which describe the complete development of an STTR Phase II effort entitled "Development of the Aerodynamic/Aeroservoelastic Modules in ASTROS". Additional aeroservoelasticity (ASE) reports are the User's Manual, the Programmer's Manual, and the Application Manual.				
14. SUBJECT TERMS Multidisciplinary Optimization, Aeroelasticity, Aeroservoelasticity, Gust Response, ASTROS			15. NUMBER OF PAGES 73	
			16. PRICE CODE	
17. SECURITY CLASSIFICATION OF REPORT UNCLASSIFIED	18. SECURITY CLASSIFICATION OF THIS PAGE UNCLASSIFIED	19. SECURITY CLASSIFICATION OF ABSTRACT UNCLASSIFIED	20. LIMITATION OF ABSTRACT SAR	

FOREWORD

This final report is submitted in fulfillment of CDRL CLIN 0001, Data Item A001, Title: Scientific and Technical Reports of a Small business Technology Transfer (STTR) Phase II contract No. F33615-96-C-3217 entitled, "Development of the Aerodynamic/Aeroservoelastic Modules in ASTROS," covering the performance period from 24 September 1996 to 24 September 1998.

This work is the second phase of a continuing two-phase STTR contract supported by AFRL/Wright-Patterson. The first phase STTR contract No. F33615-95-C-3219 entitled, "Enhancement of the Aeroservoelastic Capability in ASTROS," was completed in May 1996 and published as WL-TR-96-3119.

Both STTR Phase I and Phase II contracts are performed by the same ZONA Team in which ZONA Technology, Inc. is the prime contractor, whereby the team members include: the University of Oklahoma (OU), Universal Analytics, Inc. (UAI), and Technion (I.T.T.).

This final report consists of eight volumes, these are:

ASTROS*

- | | | |
|------------|---|---------------------------|
| Volume I | - | ZAERO User's Manual |
| Volume II | - | ZAERO Programmer's Manual |
| Volume III | - | ZAERO Application Manual |
| Volume IV | - | ZAERO Theoretical Manual |

ASTROServo

- | | | |
|------------|---|--|
| Volume I | - | Aeroservoelastic Discipline in ASTROS, User's Manual |
| Volume II | - | Aeroservoelastic Discipline in ASTROS, Programmer's Manual |
| Volume III | - | Aeroservoelastic Discipline in ASTROS, Application Manual |
| Volume IV | - | Aeroservoelastic Discipline in ASTROS, Theoretical Manual |

This document (Volume IV) is the Theoretical Manual of the Aeroservoelastic (ASE) interaction module developed to facilitate ASE analysis and the application of ASE stability and response constraints within ASTROS.

At AFRL/Wright-Patterson, Captain Gerald Andersen was the contract monitor and Dr. V. B. Venkayya was the initiator of the whole STTR effort. The technical advice and assistance received from Mr. Doug Niell of the MacNeal Schwendler Corporation, Dr. V. B. Venkayya and others from AFRL during the course of the present phase on the development of ASTROS* are gratefully acknowledged.

Contents

1	Introduction	1
2	Generalized Matrices	3
2.1	The Modal Assumption.....	4
2.2	Modal Mass and Stiffness Matrices.....	4
2.3	Normal Modes of the Modified Structure.....	6
2.4	Generalized Dynamic Matrices.....	7
2.4.1	Dynamic equation of motion	7
2.4.2	Sensitivity of Dynamic Matrices	9
2.4.3	Integrated section loads.....	10
2.5	Aerodynamic Forces	11
3	Rational Aerodynamic Approximations	13
3.1	Minimum-State Approximation Formula	13
3.2	Weighted Least-Square Fit	15
3.3	The Unconstrained Problem	17
3.3.1	Roger's approximation.....	17
3.3.2	Minimum-state procedure.....	17
3.3.3	Integrated load coefficients.....	20
3.4	Application of Constraints	20

3.5	Data Weighting	24
3.5.1	Measures of aeroelastic importance.....	25
3.5.2	Weight scaling and modifications.....	27
3.5.3	Relative importance of modes	28
4	State-Space Aeroservoelastic Equations	30
4.1	Aeroelastic Model.....	30
4.2	Actuator Model	33
4.3	Control System Model	35
4.3.1	Control System Elements.....	37
4.3.2	Fixed Connections in the Control System Model.....	38
4.4	The ASE Model	41
4.5	System Matrix Derivatives	44
4.6	Aeroelastic System Gain and Its Sensitivities	45
5	Flutter Analysis	46
5.1	Flutter Constraints.....	46
5.2	Eigenvalue Sensitivity	47
5.3	Flutter Boundary	49
6	Control Stability Margins	51
6.1	SISO Stability Margins.....	51
6.1.1	SISO Transfer Functions from a MIMO Control System.....	52
6.1.2	SISO Gain Margins.....	54
6.1.3	SISO Phase Margins	55
6.1.4	Sensitivities of SISO Gain Margins.....	57
6.1.5	Sensitivities of SISO Phase Margins	58
6.2	MIMO Stability Margins and Sensitivities.....	59

7	Continuous Gust Response	59
7.1	Equation of Motion.....	62
7.2	Gust Model.....	65
7.3	Gust Response Analysis.....	68
7.4	Sensitivity Analysis	70
	References	71

Chapter 1

Introduction

The common approach for formulating the dynamic equations of motion of aeroelastic systems uses normal modes of the structure as generalized coordinates. Control-surface deflection modes may be added when the interaction with the control system is considered. Complex gust velocity modes may also be added to analyze the response of the structural and control systems to continuous gust. The unsteady aerodynamic force coefficients are defined with respect to these modes.

The unsteady aerodynamic codes in ASTROS assume that the structure oscillates harmonically. Transcendental unsteady aerodynamic matrices are calculated for various reduced frequency values. The flutter and gust-response modules in ASTROS use second-order formulations for stability solutions, frequency response, and frequency-domain control synthesis.

The application of various modern control design techniques, simulations and optimization procedures require the aeroservoelastic equations of motion to be transformed into a first-order, time-domain (state-space) form. This transformation requires the aerodynamic matrices to be approximated by rational functions (ratio of polynomials) in the Laplace domain. The order of the resulting state-space model is a function of the number of selected modes, the number of aerodynamic approximation roots, and the approximation formula. The main considerations in constructing the model are its size (which affects the efficiency of subsequent analyses), its accuracy, and the model construction efforts.

Most commonly used rational aerodynamic approximation methods are variations of either Roger's classic approximation [1], which is based on term-by-term least-square fits with common denominator roots, or the minimum-state (MS) method of Karpel [2, 3] which is based on a more general approximation function with coupling between terms. Consequently, the MS procedure requires computationally heavier, iterative, nonlinear least-square solutions. Recent developments of the MS method [4-8] improved the accuracy, flexibility and computational efficiency of the MS scheme. The number of aerodynamic states added by the MS method in realistic aeroelastic design models is typically 6-8 times smaller than those added by Roger's approximation with the same level of model accuracy in subsequent analyses. This makes the MS method very attractive in repetitive aeroelastic optimization studies which are based on modes of a baseline structure, and in cases which involve control synthesis.

Chapter 2

Generalized Matrices

The modal approach to structural optimization is based on using a set of low-frequency normal modes of the baseline structure as a fixed set of generalized coordinates throughout the entire optimization process, or at least for a major optimization cycle composed of several design steps. The implementation of the modal approach in ASTROS required a slight modification of this approach. Instead of keeping the modal coordinates fixed, they are changed in each design step, but the new set of modal coordinates is assumed to be a linear combination of the baseline set. Mathematically, there is no difference between the two approaches.

It is currently assumed that the model does not include extra points, such that the h-set and i-set are identical. If extra points would exist, the formulation below would apply to the ii blocks of the dynamic matrices only, with the other blocks remain unchanged during the design process. We also assume here that the contributions of the design variables to the stiffness and mass matrices are linear.

2.1 The Modal Assumption

The set of n_i calculated baseline modes $[\phi_{ai}]$, defined in the a-set structural coordinates, satisfy the eigenvalue problem

$$[K_{aa}][\phi_{ai}] = [M_{aa}][\phi_{ai}][\Omega] \quad (2.1)$$

where $[\Omega]$ is a diagonal matrix of the n_i eigenvalues. If static Guyan reduction is applied, the modes can be recovered to the f-set by

$$[\phi_{fi}] = \begin{bmatrix} I \\ G_o \end{bmatrix} [\phi_{ai}] \quad (2.2)$$

Recovery of single- and multi-point constrained displacements leads to the g- set normal modes $[\phi_{gi}]$.

The basic assumption of the modal approach is that the structural displacements during structural response to external excitation can be adequately expressed as a linear combination of the baseline modes:

$$\{u_a\} = [\phi_{ai}]\{\xi\} \quad (2.3)$$

where $\{u_a\}$ is the a-set structural displacement vector and $\{\xi\}$ is the vectors of generalized displacements.

2.2 Modal Mass and Stiffness Matrices

The discrete-coordinate g-set stiffness and mass matrices are assembled in the design loop by adding the contributions of the n_{dv} global design variables to the contribution of the elements that are not subject to changes. The assembly equations, (5-43) and (5-44) of Ref. 9, when all the structural elements are linear with respect to the design variables, can be written as

$$[K_{gg}] = [DKV]_0 + \sum_{i=1}^{n_{dv}} v_i [DKV]_i \quad (2.4)$$

where $[DKV]_i$ is a regular linear contributions of the design variable v_i . The mass matrix is assembled by

$$[M_{gg}] = [DMV]_0 + \sum_{i=1}^{n_{dv}} v_i [DMV]_i \quad (2.5)$$

The coefficient matrices in Eqs. (2.4) and (2.5) are stored in the standard ASTROS data base for subsequent sensitivity analyses.

The premultiplication of Eq. (2.4) by $[\phi_{gi}]^T$ and the postmultiplication by $[\phi_{gi}]$ yield the assembled generalized stiffness matrix

$$[K_{ii}] = [DGKV]_0 + \sum_{i=1}^{n_{dv}} v_i [DGKV]_i \quad (2.6)$$

where

$$[DGKV]_i = [\phi_{gi}]^T [DKV]_i [\phi_{gi}] \quad (2.7)$$

The rigid-body related portions of $[K_{ii}]$ are zero. The premultiplication of Eq. (2.5) by $[\phi_{gi}]^T$ and the postmultiplication by $[\phi_{gi}]$, yield the generalized mass matrix

$$[M_{ii}] = [DGMV]_0 + \sum_{i=1}^{n_{dv}} v_i [DGMV]_i \quad (2.8)$$

where

$$[DGMV]_i = [\phi_{gi}]^T [DMV]_i [\phi_{gi}] \quad (2.9)$$

A major advantage of the modal approach is that we can modify the generalized stiffness and mass matrices, due to design changes, and repeat the analysis without returning to the large-size finite-element model. When all the design variables are at their baseline values v_{b_i} , both $[K_{ii}]$ and $[M_{ii}]$ are diagonal. They are generally full in the modified structure (except for the rigid-body rows and columns in $[K_{ii}]$ which remain zero).

Denoting these baseline matrices by subscript b , we can rewrite Eqs. (2.6) and (2.8) as

$$[K_{ii}] = [K_{ii}]_b + \sum_{i=1}^{n_{dv}} (v_i - v_{b_i}) [DGKV]_i \quad (2.10)$$

and

$$[M_{ii}] = [M_{ii}]_b + \sum_{i=1}^{n_{dv}} (v_i - v_{b_i}) [\text{DGMV}]_i \quad (2.11)$$

Aeroservoelastic analysis with moving control surfaces requires the mass coupling $[M_{ic}]$ between the modal coordinates and the control surface deflection modes. For the baseline structure,

$$[M_{ic}]_b = [\text{DGMVC}]_0 + \sum_{i=1}^{n_{dv}} v_{b_i} [\text{DGMVC}]_i \quad (2.12)$$

where

$$[\text{DGMVC}]_i = [\phi_{gi}]^T [\text{DMV}]_i [\phi_{gc}] \quad (2.13)$$

where $[\phi_{gc}]$ is the matrix of g-set control modes. Each control mode contains the kinematic structural displacements due to a unit deflection of the associated control surface. The modified mass coupling matrices is and

$$[M_{ic}] = [M_{ic}]_b + \sum_{i=1}^{n_{dv}} (v_i - v_{b_i}) [\text{DGMVC}]_i \quad (2.14)$$

2.3 Normal Modes of the Modified Structure

The n_i normal modes $[\tilde{\phi}_{ai}]$ of the modified structure satisfy the eigenvalue equation

$$[K_{aa}][\tilde{\phi}_{ai}] = [M_{aa}][\tilde{\phi}_{ai}][\tilde{\Omega}] \quad (2.15)$$

where $[\tilde{\Omega}]$ is a diagonal matrix of the corresponding eigenvalues.

It is assumed that the normal modes of the modified structure are linear combinations of the baseline modes $[\phi]$ at all the discrete coordinate set levels. At the a-set level it reads

$$[\tilde{\phi}_{ai}] = [\phi_{ai}][\psi] \quad (2.16)$$

where $[\psi]$ is a square non-singular matrix. The substitution of Eq. (2.16) in Eq. (2.15) and premultiplication by $[\phi_{ai}]^T$, yields the eigenvalue problem

$$[K_{ii}][\psi] = [M_{ii}][\psi][\tilde{\Omega}] \quad (2.17)$$

where $[K_{ii}]$ is defined in Eq. (2.6) and $[M_{ii}]$ in Eq. (2.8). Eq. (2.17) can be solved for the eigenvalues $[\tilde{\Omega}]$ and the eigenvectors $[\psi]$, with $[\psi]$ normalized such that

$$[\psi]^T [M_{ii}] [\psi] = [I] \quad (2.18)$$

which yields

$$[\psi]^T [K_{ii}] [\psi] = [\tilde{\Omega}] \quad (2.19)$$

To allow the formulation below to be applicable to the baseline structure as well as the modified one, we define the baseline $[\psi]$ as

The application of Eq. (2.17) to the j -th eigenvector, $\{\psi_j\}$, its differentiation with respect to a design variable v_i , and premultiplication by $\{\psi_j\}^T$ yield the sensitivity of the j -th eigenvalue,

$$\frac{\partial \tilde{\Omega}_j}{\partial v_i} = \{\psi_j\}^T \left([DGKV]_i - \tilde{\Omega}_j [DGMV]_i \right) \{\psi_j\} \quad (2.20)$$

which can be used in calculating the frequency constraint sensitivities. In order to apply Eq. (2.20) and the generalized formulation below to the baseline structure as well as to the modified ones, the baseline modes are normalized for unit generalized masses by Eq. (2.16) with

$$[\psi]_b = [M_{ii}]_b^{-1/2} \quad (2.21)$$

2.4 Generalized Dynamic Matrices

2.4.1 Dynamic equation of motion

The generalized dynamic matrices are constructed in the h -set coordinates which are based on the i -set modes plus extra (e-set) user-defined coordinates. As mention above, the formulation below assumes that there are no extra degrees of freedom, such that $n_h = n_i$. However,

while i-set matrices are related in this document to the baseline modes $[\phi_{ai}]$, h-set matrices are related to the modified modes

$$[\phi_{ah}] = [\tilde{\phi}_{ai}] = [\phi_{ai}][\psi] \quad (2.22)$$

where $[\phi_{ai}]$ is kept fixed and $[\phi_{ah}]$ varies during the optimization according to $[\psi]$. Another difference between the h-set and the i-set matrices is that, like in the standard ASTROS, the h-set matrices include the effects of direct-input structural matrices $[M_{gg}^2]$, $[K_{gg}^2]$ and $[B_{gg}^2]$ which are not included in the eigenvalue analysis and are not subject to changes in the design process.

The time-domain matrix equation of motion in modal coordinates is

$$[M_{hh}]\{\ddot{\xi}\} + [B_{hh}]\{\dot{\xi}\} + [K_{hh}]\{\xi\} = \{P_h(t)\} \quad (2.23)$$

where the generalized mass and stiffness matrices are

$$[K_{hh}] = [\psi]^T \left([K_{ii}] + [K_{ii}^2] \right) [\psi] = [\tilde{\Omega}] + [\psi]^T [K_{ii}^2] [\psi] \quad (2.24)$$

and

$$[M_{hh}] = [\psi]^T \left([M_{ii}] + [M_{ii}^2] \right) [\psi] = [I] + [\psi]^T [M_{ii}^2] [\psi] \quad (2.25)$$

where

$$[M_{ii}^2] = [\phi_{gi}]^T [M_{gg}^2] [\phi_{gi}]; \quad [K_{ii}^2] = [\phi_{gi}]^T [K_{gg}^2] [\phi_{gi}]$$

The generalized damping matrix is based on the regular damping options in ASTROS, with some modifications,

$$[B_{hh}] = [g(\omega_h)][\omega_h] + [\psi]^T [B_{ii}^2] [\psi] + \frac{g}{\omega_3} [\tilde{\Omega}] \quad (2.26)$$

where

$$[B_{ii}^2] = [\phi_{gi}]^T [B_{gg}^2] [\phi_{gi}]$$

and $[\omega_h] = [\tilde{\Omega}]^{1/2}$. The optional user-input damping parameters here are those used in the standard ASTROS, namely the general structural damping g , ω_3 which defines the equivalent viscous damping, and the modal damping table $g(\omega_h)$.

The excitation vector in Eq. (2.22), $\{P_h\}$, can contain prescribed external inputs, aerodynamic forces which are discussed in the following section, and inertial forces due to control commands. The generalized forces due to prescribed external excitation are

$$\{P_h^p\} = [\phi_{gh}]^T \{F(t)\} \quad (2.27)$$

The inertial forces due to control surface accelerations are

$$\{P_h^i\} = -[M_{hc}]\{\ddot{\delta}_c\} \quad (2.28)$$

where

$$[M_{hc}] = [\psi]^T ([M_{ic}] + [M_{ic}^2]) \quad (2.29)$$

where

$$[M_{ic}^2] = [\phi_{gi}]^T [M_{gg}^2] [\phi_{gc}]$$

2.4.2 Sensitivity of Dynamic Matrices

The change of modal coordinates (by changing $[\psi]$) in each design iteration complicates the sensitivity analysis compared to that of the fixed-basis analysis. To allow simple expressions, the sensitivity analysis in each iteration assumes that the dynamic matrices of the next iteration will be based on the current modal coordinates. Consequently, the differentiation of $[K_{hh}]$ and $[M_{hh}]$ with respect to the design variables are based on Eqs. (2.25) and (2.24) with fixed $[\psi]$, $[K_{ii}^2]$ and $[M_{ii}^2]$, and variable $[K_{ii}]$ $[M_{ii}]$. The resulting sensitivities are

$$\frac{\partial}{\partial v_i} [K_{hh}] = [\psi]^T [\text{DGKV}]_i [\psi] \quad (2.30)$$

and

$$\frac{\partial}{\partial v_i} \begin{bmatrix} M_{hh} & M_{hc} \end{bmatrix} = [\psi]^T \begin{bmatrix} \text{DGMV}_i \psi & \text{DGMVC}_i \end{bmatrix} \quad (2.31)$$

2.4.3 Integrated section loads

Section loads due to aeroelastic response are calculated by the summation-of-force approach which adds the effects of aerodynamic, inertial and prescribed forces. The effects of the prescribed forces are

$$\{P_L^p\} = [\phi_{gL}]^T \{F(t)\} \quad (2.32)$$

where $[\phi_{gL}]$ is the matrix of integration load modes. Each load mode contains the kinematic structural displacements due to a unit displacement of a reference degree of freedom defined by the user. The inertial parts of the section loads can be calculated by

$$\{P_L^i\} = -[M_{Lh}]\{\ddot{\xi}\} - [M_{Lc}]\{\ddot{\delta}_c\} \quad (2.33)$$

where the mass matrices are first defined by

$$\begin{bmatrix} M_{Li} & M_{Lc} \end{bmatrix}_b = [\phi_{gL}]^T \left([M_{gg}] + [M_{gg}^2] \right) \begin{bmatrix} \phi_{gi} & \phi_{gc} \end{bmatrix} \quad (2.34)$$

and then updated by

$$\begin{bmatrix} M_{Li} & M_{Lc} \end{bmatrix} = \begin{bmatrix} M_{Li} & M_{Lc} \end{bmatrix}_b + \sum_{i=1}^{n_{dv}} (v_i - v_{b_i}) \begin{bmatrix} \text{DGMVLI}_i & \text{DGMVLC}_i \end{bmatrix} \quad (2.35)$$

from which $[M_{Lh}]$ is calculated by

$$[M_{Lh}] = [M_{Li}][\psi] \quad (2.36)$$

Following the sensitivity formulation above, the derivatives of the mass matrices associated with the section loads are

$$\frac{\partial}{\partial v_i} \begin{bmatrix} M_{Lh} & M_{Lc} \end{bmatrix} = \begin{bmatrix} \text{DGMVLI}_i \psi & \text{DGMVLC}_i \end{bmatrix} \quad (2.37)$$

2.5 Aerodynamic Forces

The unsteady aerodynamic routines in ASTROS assume that the structure undergoes harmonic oscillations. Complex aerodynamic force coefficient (AFC) matrices (at a given Mach number) for n_ℓ user-defined "tabulated" values of the reduced frequency $k = \omega b/V$ where ω is the frequency of oscillations and b is a reference semichord. These complex AFC matrices, $[Q_{kk}(ik_\ell)]$ are stored in a data base for subsequent analyses. Their dimension is $n_k \times n_k$ where n_k is the number of aerodynamic degrees of freedom. The ZAERO unsteady aerodynamic module also calculates the coefficient matrices $[Q_{kc}(ik_\ell)]$, $[Q_{kg}(ik_\ell)]$, $[Q_{Lk}(ik_\ell)]$, $[Q_{Lc}(ik_\ell)]$ and $[Q_{LG}(ik_\ell)]$ in the following generalized force expressions. These matrices are independent of the structural properties.

The generalized unsteady aerodynamic forces acting on the structural modes of a linear aeroelastic system can be expressed in the frequency domain as:

$$\{P_h^a(i\omega)\} = -q[Q_{hh}(ik)]\{\xi(i\omega)\} - q[Q_{hc}(ik)]\{\delta_c(i\omega)\} - \frac{q}{V}[Q_{hG}(ik)]\{w_G(i\omega)\} \quad (2.38)$$

where q is the dynamic pressure, V is the true air velocity, and $\{\xi\}$, $\{\delta_c\}$ and $\{w_G\}$ are the vectors of n_h generalized structural displacements, n_c control surface commanded deflections (actuator outputs), and n_G gust velocities. $[Q_{hh}]$, $[Q_{hc}]$ and $[Q_{hG}]$ are the associated generalized unsteady aerodynamic force coefficient matrices calculated by

$$\begin{bmatrix} Q_{hh} & Q_{hc} & Q_{hG} \end{bmatrix} = [\phi_{kh}]^T \begin{bmatrix} Q_{kk}\phi_{kh} & Q_{kc} & Q_{kG} \end{bmatrix} \quad (2.39)$$

where

$$[\phi_{kh}] = [G_{kf}][\phi_{fh}]$$

where $[G_{kf}]$ is the spline matrix.

The unsteady aerodynamic section loads are

$$\{P_L^a(i\omega)\} = -q[Q_{Lh}(ik)]\{\xi(i\omega)\} - q[Q_{Lc}(ik)]\{\delta_c(i\omega)\} - \frac{q}{V}[Q_{LG}(ik)]\{w_G(i\omega)\} \quad (2.40)$$

where $[Q_{Lh}]$ is calculated by

$$[Q_{Lh}] = [Q_{Lk}][\phi_{kh}] \quad (2.41)$$

Once calculated for the baseline structure with the original modes $[\phi_{ki}]$, the generalized force coefficient matrices are updated during the optimization by

$$\begin{bmatrix} Q_{hh} & Q_{hc} & Q_{hG} \\ Q_{Lh} & Q_{Lc} & Q_{LG} \end{bmatrix} = \begin{bmatrix} \psi^T Q_{ii} \psi & \psi^T Q_{ic} & \psi^T Q_{iG} \\ Q_{Li} \psi & Q_{Lc} & Q_{LG} \end{bmatrix} \quad (2.42)$$

Chapter 3

Rational Aerodynamic Approximations

Rational aerodynamic approximations (RAA) are required in order to cast the dynamic aeroelastic equation of motion in a state-space form. The approximation options described in this chapter should be selected for best combination of accuracy and efficiency in subsequent stability and response analyses.

The approximations are constructed for the baseline model with the aerodynamic data associated with the original modes $[\phi_{ai}]$. Nevertheless, the subscripts of the generalized aerodynamic matrices in this chapter are denoted by h instead of i for consistency with the notations in other documents. The resulting approximation matrices remain unchanged, except multiplication by normalization matrices (see Chapter 4), throughout the optimization process, in all the ASE disciplines.

3.1 Minimum-State Approximation Formula

The generalized unsteady aerodynamic forces in Eqs. (2.38) and (2.40) can be expressed in the Laplace s domain as:

$$\begin{Bmatrix} P_h^a(s) \\ P_L^a(s) \end{Bmatrix} = -q \begin{bmatrix} Q_{hh}(s) \\ Q_{Lh}(s) \end{bmatrix} \{\xi(s)\} - q \begin{bmatrix} Q_{hc}(s) \\ Q_{Lc}(s) \end{bmatrix} \{\delta_c(s)\} - \frac{q}{V} \begin{bmatrix} Q_{hG}(s) \\ Q_{LG}(s) \end{bmatrix} \{w_G(s)\} \quad (3.1)$$

The AFC matrices are normally not available as explicit functions of s . In order to cast the aeroelastic equation of motion in a time-domain constant coefficient equation, the AFC matrices have to be described as rational functions of s . The most general rational function approximation of the merged AFC matrices

$$[Q(s)] = \begin{bmatrix} Q_h \\ Q_L \end{bmatrix} = \begin{bmatrix} Q_{hh} & Q_{hc} & Q_{hG} \\ Q_{Lh} & Q_{Lc} & Q_{LG} \end{bmatrix}$$

that leads to a state-space aeroelastic model can be cast in the form

$$\begin{bmatrix} \tilde{Q}_h(p) \\ \tilde{Q}_L(p) \end{bmatrix} = \begin{bmatrix} A_{h0} \\ A_{L0} \end{bmatrix} + \begin{bmatrix} A_{h1} \\ A_{L1} \end{bmatrix} p + \begin{bmatrix} A_{h2} \\ A_{L2} \end{bmatrix} p^2 + \begin{bmatrix} D_h \\ D_L \end{bmatrix} ([I]p - [R])^{-1} [E]p \quad (3.2)$$

where p is the nondimensional complex Laplace variable $p = sb/V$ and all the matrix coefficients are real valued [2]. The common $[R]$ and $[E]$ facilitates the formulation of section loads as output variables in the state-space aeroelastic equations of motion. The number of structural states in the resulting state-space model is $2n_h$. The number of aerodynamic states (n_a) is equal to the order of the aerodynamic root matrix $[R]$.

Since the aerodynamic data is given for harmonic oscillations, the approximation process starts with the replacement of p in Eq. (3.2) by ik , where k is the nondimensional frequency $\omega b/V$. Least-square procedures are then used to calculate the approximation coefficients that best fit the tabulated $[Q(ik_l)]$ matrices.

Roger [1] dealt with $[Q_h]$ only. He approximated each aerodynamic term $[Q_h(ik)]$ separately, but with n_l common aerodynamic roots,

$$[\tilde{Q}_h(ik)] = [A_{h0}] + ik[A_{h1}] - k^2[A_{h2}] + \sum_{l=3}^{n_l+2} \frac{ik}{ik + \gamma_{l-2}} [A_{hl}] \quad (3.3)$$

which can be cast in the form of Eq. (3.2) with

$$[D_h] = \begin{bmatrix} I & I & \cdots \end{bmatrix}, \quad [R] = - \begin{bmatrix} \gamma_1 I & & \\ & \gamma_2 I & \\ & & \ddots \end{bmatrix}, \quad [E] = \begin{bmatrix} A_{h3} \\ A_{h4} \\ \vdots \end{bmatrix} \quad (3.4)$$

which implies that the resulting number of aerodynamic states is $n_a = n_l \times n_h$.

Equation (3.4) shows that Roger treated the elements of $[E]$ as free variables in the approximation process, while those of $[D_h]$ were fixed, and that $[R]$ has repeated roots. The MS method [2, 3] was based on the realization that the number of aerodynamic states per desired accuracy can be reduced significantly by treating all the elements of both $[D_h]$ and $[E]$ as free variables, and by letting the diagonal $[R]$ be with distinct negative roots. The number of MS distinct roots, n_l , and their values are defined by the analyst. This number is typically larger than that in Roger's approximation, but the number of resulting aerodynamic states, $n_a = n_l$ is much smaller. Typical MS applications [4-6] used 4 to 6 roots with the span of their absolute values similar to that of the tabulated reduced frequencies. The MS applications showed small sensitivity to the root values.

3.2 Weighted Least-Square Fit

To facilitate real-valued algebra, the complex approximation expression in Eq. (3.2), with p replaced by ik , is separated into real and imaginary parts. The real part of the h partition is

$$[\tilde{F}_h(k)] = [A_{h0}] - k^2[A_{h2}] + k^2[D_h][K(k)][E] \quad (3.5)$$

where

$$[K(k)] = (k^2[I] + [R]^2)^{-1}$$

is diagonal, and the imaginary part is

$$[\tilde{G}_h(k)] = k[A_{h1}] - k[D_h][K(k)][R][E] \quad (3.6)$$

The L partition of Eq. (3.2) is expressed by Eqs. (3.5) and (3.6) with subscript h replaced by L . It can be noticed that both $[\tilde{Q}_h]$ and $[\tilde{Q}_L]$ use the same $[R]$, $[K(k)]$ and $[E]$ matrices.

The comparison of Eqs. (3.5) and (3.6) with the real and imaginary parts, $[F(k_\ell)]$ and $[G(k_\ell)]$, of the tabulated AFC matrices $[Q(ik_\ell)]$ provides an overdetermined set of approximate equations. The task is to find the free approximation coefficients in $[A_0]$, $[A_1]$, $[A_2]$, $[D]$ and $[E]$ that minimize, under some constraints, the total least-square approximation error

$$\varepsilon_t = \sqrt{\sum_{i,j,\ell} |\tilde{Q}_{ij}(ik_\ell) - Q_{ij}(ik_\ell)|^2 W_{ij\ell}^2} \quad (3.7)$$

where $W_{ij\ell}$ is the weight assigned to the ij -th term of the ℓ -th tabulated AFC matrix. The weight options in Eq. (3.7) are discussed in Section 3.5.

For numerical efficiency, it is desired to decompose the overall least-square problem into a sequence of small-size standard least-square problems, each based on the general approximate equation

$$[W^*]_\ell [A^*]_\ell \{x^*\} \approx [W^*]_\ell \{b^*\}_\ell \quad \text{for } \ell = 1, n_k \quad (3.8)$$

where $\{x^*\}$ is a subset of unknown coefficients which are uncoupled with others, $\{b^*\}_\ell$ is extracted from the tabulated data, and $[A^*]_\ell$ is a function of k_ℓ , the aerodynamic root values and the constraints associated with unknowns, as detailed below for the various techniques. The weight matrix $[W^*]_\ell$ is a diagonal matrix whose terms are the weights $W_{ij\ell}$ associated with data terms in $\{b^*\}_\ell$. The weighted least-square solution for $\{x^*\}$ is obtained by solving the symmetric problem

$$[C]\{x^*\} = \{b\} \quad (3.9)$$

where

$$\begin{aligned} [C] &= \sum_{\ell} [A^*]_\ell^T [W^*]_\ell^2 [A^*]_\ell \\ \{b\} &= \sum_{\ell} [A^*]_\ell^T [W^*]_\ell^2 \{b^*\}_\ell \end{aligned}$$

Various approximation cases are presented in Sections 3.3 and 3.4 by defining their sequence of least-square solutions, the unknown coefficients $\{x^*\}$ in each solution, and the associated

data vectors $\{b^*\}_l$ and approximation matrices $[A^*]_l$ of Eq. (3.8). The weight are discussed in Section 3.5.

3.3 The Unconstrained Problem

The approximation coefficients of Eq. (3.2) are determined by solving a sequence of weighted least-square problems. The coefficients of $[\tilde{Q}_h]$ are determined by either Roger's or the MS procedures. The coefficients of $[\tilde{Q}_L]$ are then defined with $[E]$ of the $[\tilde{Q}_h]$. The diagonal $[R]$ is defined by the user in all the cases.

3.3.1 Roger's approximation

The structure of Eq. (3.3) indicates that the coefficients of Roger's approximation can be found for each aerodynamic term separately by performing $n_h \times (n_h + n_c + n_G)$ solutions of Eq. (3.9) with

$$[A^*]_l = \begin{bmatrix} 1 & 0 & -k_l^2 & \frac{k_l^2}{k_l^2 + \gamma_1^2} & \frac{k_l^2}{k_l^2 + \gamma_2^2} & \dots \\ 0 & k_l & 0 & \frac{k_l \gamma_1}{k_l^2 + \gamma_1^2} & \frac{k_l \gamma_2}{k_l^2 + \gamma_2^2} & \dots \end{bmatrix}, \quad \{x^*\} = \begin{bmatrix} A_{h0ij} \\ A_{h1ij} \\ \vdots \end{bmatrix}, \quad \{b^*\}_l = \begin{bmatrix} F_{hij}(k_l) \\ G_{hij}(k_l) \end{bmatrix} \quad (3.10)$$

where the number of unknowns in each solution is $n_l + 3$. The right-side terms, F_{hij} and G_{hij} are the real and imaginary parts of the (i, j) term of $[Q_h(ik_l)]$. The resulting $\{x^*\}$ vectors and the user-input lag term γ_l are used to define the coefficient matrices in Eqs. (3.3) and (3.4).

3.3.2 Minimum-state procedure

With both $[D_h]$ and $[E]$ in Eq. (3.2) being unknown, the MS problem for a given $[R]$ is nonlinear. It is solved iteratively by starting with an initial guess of $[D_h]$ in which at least one term in each row and each column is nonzero. For a given $[D_h]$, Eqs. (3.5) and (3.6)

imply that the unknown MS coefficient matrices $[A_{h0}]$, $[A_{h1}]$, $[A_{h2}]$ and $[E]$ can be calculated by performing $n_h + n_c + n_G$ column-by-column solutions of Eq.(3.9) with

$$[A^*]_l = \begin{bmatrix} I & 0 & -k_l^2 I & k_l^2 D_h K(k_l) \\ 0 & k_l I & 0 & -k_l D_h K(k_l) R \end{bmatrix}, \quad \{x^*\} = \begin{Bmatrix} A_{h0j} \\ A_{h1j} \\ A_{h2j} \\ E_j \end{Bmatrix}, \quad \{b^*\}_l = \begin{Bmatrix} F_{hj}(k_l) \\ G_{hj}(k_l) \end{Bmatrix} \quad (3.11)$$

where the j indices relate to the j -th columns of the respective matrices. The number of unknowns in each regular solution is $3n_h + n_l$. The calculated $[E]$ is then used to update $[A_{h0}]$, $[A_{h1}]$, $[A_{h2}]$ and $[D_h]$ by performing n_h row-by-row solutions of Eq. (3.9) with

$$[A^*]_l = \begin{bmatrix} I & 0 & -k_l^2 I & k_l^2 E^T K(k_l) \\ 0 & k_l I & 0 & -k_l E^T K(k_l) R \end{bmatrix}, \quad \{x^*\} = \begin{Bmatrix} A_{h0i}^T \\ A_{h1i}^T \\ A_{h2i}^T \\ D_{hi}^T \end{Bmatrix}, \quad \{b^*\}_l = \begin{Bmatrix} F_{hi}^T(k_l) \\ G_{hi}^T(k_l) \end{Bmatrix} \quad (3.12)$$

where the i indices relate to the i -th rows of the respective matrices. The number of unknowns in each solution of Eq. (3.12) is $3(n_h + n_c + n_G) + n_l$. The least-square solutions with Eqs. (3.11) and (3.12) form a $D \rightarrow E \rightarrow D$ iteration which is repeated until convergence is obtained or until a specified maximum number of iterations is reached.

The iterative nature of the MS procedure, and the relatively large number of unknowns solved for simultaneously in each iteration of the regular unconstrained problem, require a considerably larger computation time than that of Roger's method. A major reduction in the MS computation efforts was obtained in Refs. [2-7] by applying 3 approximation constraints. The efficient solution of Eq. (3.9) presented in Ref. [8] allows similar computational savings without having to apply constraints. It can be observed that the structure of the least-square equation (3.9) with the coefficients and variables of Eq. (3.11) is:

$$\begin{bmatrix} C_{11} & 0 & C_{13} & C_{14} \\ 0 & C_{22} & 0 & C_{24} \\ C_{13} & 0 & C_{33} & C_{34} \\ C_{14}^T & C_{24}^T & C_{34}^T & C_{44} \end{bmatrix} \begin{Bmatrix} A_{h0j} \\ A_{h1j} \\ A_{h2j} \\ E_j \end{Bmatrix} = \begin{Bmatrix} b_1 \\ b_2 \\ b_3 \\ b_4 \end{Bmatrix} \quad (3.13)$$

where $[C_{11}]$, $[C_{22}]$, $[C_{13}]$ and $[C_{33}]$ are diagonal. This structure facilitates an efficient solution of Eq. (3.13) through a sequential reduction of the problem size. The first row of Eq. (3.13) yields:

$$\{A_{h0,j}\} = [C_{11}]^{-1} \left(\{b_1\} - [C_{13}]\{A_{h2,j}\} - [C_{14}]\{E_j\} \right) \quad (3.14)$$

The substitution of Eq. (3.14) in rows 2 to 4 of Eq. (3.13) yields:

$$\begin{bmatrix} C_{22} & 0 & C_{24} \\ 0 & \bar{C}_{33} & \bar{C}_{34} \\ C_{24}^T & \bar{C}_{34}^T & \bar{C}_{44} \end{bmatrix} \begin{Bmatrix} A_{h1,j} \\ A_{h2,j} \\ E_j \end{Bmatrix} = \begin{Bmatrix} b_2 \\ \bar{b}_3 \\ \bar{b}_4 \end{Bmatrix} \quad (3.15)$$

where $[C_{22}]$ and $[\bar{C}_{33}]$ remain diagonal. The next step is the extraction of $\{A_{h1,j}\}$ and $\{A_{h2,j}\}$ from the first two rows of Eq. (3.15), and their substitution in the third row. The result is

$$[\tilde{C}]\{E_j\} = \{\tilde{b}\} \quad (3.16)$$

where

$$\begin{aligned} [\tilde{C}] &= \bar{C}_{44} - C_{24}^T C_{22}^{-1} C_{24} - \bar{C}_{34}^T \bar{C}_{33}^{-1} \bar{C}_{34} \\ \{\tilde{b}\} &= \bar{b}_4 - C_{24}^T C_{22}^{-1} b_2 - \bar{C}_{34}^T \bar{C}_{33}^{-1} \bar{b}_3 \end{aligned}$$

Equation (3.16) is of order n_l only, with symmetric $[\tilde{C}]$. The diagonality of $[C_{11}]$ and $[C_{13}]$ in Eq. (3.14), and $[C_{22}]$ and $[\bar{C}_{33}]$ in Eq. (3.15) implies that the reduction of $\{A_{h0,j}\}$, $\{A_{h1,j}\}$ and $\{A_{h2,j}\}$ does not involve matrix inversion and can be performed term by term. The reduction of the i -th row in $\{A_{h0,j}\}$, $\{A_{h1,j}\}$ and $\{A_{h2,j}\}$ affects only the i -th row and i -th column in $[\bar{C}_{44}]$.

The construction and solution of Eq. (3.16) are repeated until the entire $[E]$ is found for the last calculated $[D_h]$. For each $\{E_j\}$ we can use Eq. (3.15) for $\{A_{h1,j}\}$ and $\{A_{h2,j}\}$, and then Eq. (3.14) for $\{A_{h0,j}\}$. This recovery is required, however, only at the end of the iterative process, unless we want to monitor the approximation error of Eq. (3.7) during the iterative process. The same reduction and solution process can be performed for $[A_{h0}]$,

$[A_{h1}]$, $[A_{h2}]$ and $[D_h]$, this time row by row, with the coefficients of Eq. (3.12) using the last calculated $[E]$.

The sequence of least-square solutions is such that, theoretically, the total error should never increase when the process progresses. However, numerical difficulties may cause it to increase when high-order approximations are applied with insufficient amount of data [6]. As demonstrated in the numerical example of Ref. [8], the reduction process reduces the solution time of a typical unconstrained problem by more than 80%.

3.3.3 Integrated load coefficients

The coefficients of $[\tilde{Q}_L]$ in Eq. (3.2) are calculated by a direct least-square solution with the $[E]$ of the $[\tilde{Q}_h]$ approximation. Equation (3.9) is solved n_L times (once for each required integrated load) with the coefficients and variables of Eq. (3.12), with subscripts h in $\{x^*\}$ and $\{b^*\}_l$ replaced by L .

When Roger's approximation is used, the resulting $[D_L]$ is an $n_L \times (n_h * n_l)$ matrix and $[Q_L]$ is approximated with $[R]$ and $[E]$ of Eq. (3.4). With MS approximation the size of $[D_L]$ is $n_L \times n_l$ and $[Q_L]$ is approximated with $[R]$ and $[E]$ of $[\tilde{Q}_h]$.

3.4 Application of Constraints

Reference [5] presented the various options in the 3-constraint MS procedure, in which 3 constraints have to be assigned to each aerodynamic term even if they are not desired. Here, when they are not required, it is still often desired to obtain exact fits at specified reduced frequencies or to null out some coefficients. The most frequently used constraint is a match of the steady-aerodynamics data (at $k = 0$). An imaginary-part data-match constraint at a k close to 0 yields $\partial \tilde{G}_{ij} / \partial k$ at $k = 0$, which affects the quasi-steady aerodynamic damping, to be equal to that of the tabulated data. Data-match constraints at higher k values are sometimes desired to increase the accuracy of anticipated flutter mechanisms. Even with

the reduction technique shown above, up to 3 constraints can be applied in a way that saves some computation time. On the other hand, it always increases the total fit errors, and sometimes causes unwanted wiggling of the resulting curve fits near the data-match points [6].

The constraint formulation is given below for the approximation of $[Q_h]$, but is applicable to the terms of $[Q_L]$ as well. The optional constraints that, when applied, reduce the approximation problem size are:

1. Steady aerodynamics match enforced in Eq. (3.5) by setting

$$A_{h0ij} = F_{hi_j}(0) \quad (3.17)$$

2. Either imaginary-part match at a nonzero $k = k_g$ enforced in Eq. (3.6) by setting

$$A_{h1ij} = \frac{1}{k_g} G_{hi_j}(k_g) + D_{hi} K(k_g) R E_j \quad (3.18)$$

or

$$A_{h1ij} = 0 \quad (3.19)$$

3. Either real-part match at a nonzero $k = k_f$ enforced in Eq. (3.5) by setting

$$A_{h2ij} = \frac{1}{k_f^2} (A_{h0ij} - F_{hi_j}(k_f)) + D_{hi} K(k_f) E_j \quad (3.20)$$

or

$$A_{h2ij} = 0 \quad (3.21)$$

Each optional constraint in Eqs. (3.17) thru (3.21) can be applied for a different subset of aerodynamic terms, not necessarily for all (i, j) terms uniformly as done in previous developments [4-6]. Different aerodynamic terms can be assigned with different match frequencies, namely different k_g and k_f values in Eqs. (3.18) and (3.20), while some of them

are constrained by Eq. (3.17) and the others are not. A definition of the default constraint set is requested in the ASE module. Other constraint sets that replace the default set can be assigned to selected columns of $[Q_h]$ and $[Q_L]$.

The constraints are applied in the approximate equation level, Eq. (3.8), by eliminating terms from $\{x^*\}$ and changing $[A^*]_t$ and $\{b^*\}_t$ accordingly. This is done before the construction of Eq. (3.9). The process is described below with the unconstrained $\{x^*\}$, $[A^*]_t$ and $\{b^*\}_t$ of Eq. (3.11) or Eq. (3.12) being the starting point.

The application of the steady aerodynamics constraints of Eq. (3.17) eliminates the i -th term in $\{A_{h0_j}\}$, and the associated column in $[A^*]_t$, and replaces $F_{h_{ij}}(k_t)$ in $\{b^*\}$ by

$$\bar{F}_{h_{ij}}(k_t) = F_{h_{ij}}(k_t) - F_{h_{ij}}(0) \quad (3.22)$$

The application of the imaginary-part constraint of either Eq. (3.18) or Eq. (3.19) eliminates the i -th term in $\{A_{1_j}\}$, and the associated column in $[A^*]_t$. The match constraint of Eq. (3.18) also replaces the i -th row of the block $[-k_t D_h K(k_t) R]$ in $[A^*]_t$ by $[-k_t D_{h_i} K_g(k_t) R]$ where

$$[K_g(k_t)] = [K(k_t)] - [K(k_g)] \quad (3.23)$$

and the $G_{h_{ij}}(k_t)$ term in $\{b^*\}$ is replaced in this case by

$$\bar{G}_{h_{ij}}(k_t) = G_{h_{ij}}(k_t) - \frac{k_t}{k_g} G_{h_{ij}}(k_g) \quad (3.24)$$

The application of the real-part constraint of either Eq. (3.20) or Eq. (3.21) eliminates the i -th term from $\{A_{h2_j}\}$, and the associated column from $[A^*]_t$. The match constraint of Eq. (3.20) also replaces the i -th row of the block $[k_t^2 D_h K(k_t)]$ in $[A^*]_t$ by $[k_t^2 D_{h_i} K_f(k_t)]$ where

$$[K_f(k_t)] = [K(k_t)] - [K(k_f)] \quad (3.25)$$

When Eq. (3.20) is applied together with Eq. (3.17), $F_{h_{ij}}(k_\ell)$ of $\{b^*\}$ is replaced by

$$\bar{F}_{h_{ij}}(k_\ell) = F_{h_{ij}}(k_\ell) - F_{h_{ij}}(0) - \frac{k_\ell^2}{k_f^2} (F_{h_{ij}}(k_f) - F_{h_{ij}}(0)) \quad (3.26)$$

Otherwise, when Eq. (3.20) is applied but Eq. (3.17) is not, $F_{h_{ij}}(k_\ell)$ becomes

$$\bar{F}_{h_{ij}}(k_\ell) = F_{h_{ij}}(k_\ell) - \frac{k_\ell^2}{k_f^2} F_{h_{ij}}(k_f) \quad (3.27)$$

and term (i, i) in $[A^*]_\ell$ is replaced by

$$\bar{I}_{ii} = 1 - \frac{k_\ell^2}{k_f^2} \quad (3.28)$$

The application of constraints to the coefficients of Eq. (3.12) is similar to that shown above for Eq. (3.11). When the three data-match constraints of Eqs. (3.17), (3.18) and (3.20) are applied simultaneously to all the (i, j) terms, and when all the terms are assigned with the same match frequencies k_g and k_f , the least-square matrices in Eq. (3.11) are reduced to

$$[A^*]_\ell = \begin{bmatrix} k_\ell^2 D_h K_f(k_\ell) \\ -k_\ell D_h K_g(k_\ell) R \end{bmatrix}, \quad \{x^*\} = \{E_j\}, \quad \{b^*\}_\ell = \begin{Bmatrix} \bar{F}_{h_j}(k_\ell) \\ \bar{G}_{h_j}(k_\ell) \end{Bmatrix} \quad (3.29)$$

where $\bar{F}_{h_{ij}}(k_\ell)$ and $\bar{G}_{h_{ij}}(k_\ell)$ are defined in Eqs. (3.26) and (3.24) respectively, and Eq. (3.12) is reduced to

$$[A^*]_\ell = \begin{bmatrix} k_\ell^2 E^T K_f(k_\ell) \\ -k_\ell E^T K_g(k_\ell) R \end{bmatrix}, \quad \{x^*\} = \{D_{h_i}^T\}, \quad \{b^*\}_\ell = \begin{Bmatrix} \bar{F}_{h_i}^T(k_\ell) \\ \bar{G}_{h_i}^T(k_\ell) \end{Bmatrix} \quad (3.30)$$

Since constraints are applied in the approximate equation level, Eq. (3.8), and the reduction process in Eqs. (3.13-3.16) is performed in the solution level, all constraints have to be applied before the reduction starts. It is clear from the previous section that constraints can be applied selectively with each aerodynamic term having a different number and type of constraints. To summarize the solution process, a single $D \rightarrow E \rightarrow D$ iteration in MS approximation of $[Q_h]$ is performed in the following steps:

1. Construction of $[A^*]_l$ and $\{b^*\}_l$ of Eq. (3.11), with selected constraints from Eqs. (3.17-3.21), for the $j = 1$ column of $[\tilde{Q}_h(p)]$ in Eq. (3.2).
2. Construction of $[C]$ of Eq. (3.9) for this column, whose terms correspond to $\{E_j\}$ and to the terms in $\{A_{h0,j}\}$, $\{A_{h1,j}\}$ and $\{A_{h2,j}\}$ that were not constrained in step 1.
3. Reduction of $[C]$ to obtain $[\tilde{C}]$ of Eq. (3.16), and solution of Eq. (3.16) for $\{E_j\}$.
4. Repetition of steps 1-3 for $j = 2, n_h + n_c + n_G$ to calculate the entire $[E]$.
5. Application of steps 1-4 to the calculation of $[D_h]$ row by row, starting with the coefficients of Eq. (3.12).
6. Recovery of the constrained terms in $[A_{h0}]$, $[A_{h1}]$ and $[A_{h2}]$ by Eqs. (3.17-3.21), and the unconstrained terms by Eqs. (3.14) and (3.15).

With Roger's approximation, steps 1-4 and 6 are performed once, starting with Eq. (3.10). To approximate $[Q_L]$, only a single $E \rightarrow D$ iteration is performed.

3.5 Data Weighting

Least-square curve fitting tends to produce smaller percentage errors at data points of large numerical values. However, large numerical values do not always reflect the actual importance of accurate fit of an element in the aerodynamic matrices. To eliminate the effect of the way the structural normal modes are normalized, they are normalized to unit generalized mass before the generalized aerodynamic matrices are calculated. The weighting in the least-square problem, Eq. (3.8), can be either uniform, with all $W_{ijl} = 1$, or based on the automatic physical weighting process [4] whose expressions are given below. The physical weighting can be applied only to the aerodynamic terms which appear in the dynamic equation of motion, namely $[Q_h]$.

3.5.1 Measures of aeroelastic importance

The physical-weighting algorithm developed in [4-6] was designed to weight each term of the tabulated data such that the magnitude of the weighted term, Eq. (3.36), indicates its "aeroelastic importance". The idea is that the weight assigned to a data term should be proportional to the estimated effect of a unit approximation error on a representative aeroelastic property. Different representative properties are selected below for the structural, control and gust-related partitions of the $[Q_h(ik\ell)]$ matrices. The error effects are estimated by the differentiation of the selected aeroelastic properties with respect to the aerodynamic terms.

The measures of aeroelastic importance are based on the frequency-domain equilibrium equation

$$[C_{hh}(ik)]\{\xi(ik)\} = \left([M_{hc}]_b \frac{k^2 V^2}{b^2} - q[Q_{hc}(ik)] \right) \{\delta_c(ik)\} - \frac{q}{V} [Q_{hG}(ik)] \{w_G(ik)\} \quad (3.31)$$

where

$$[C_{hh}(ik)] = -[M_{ii}]_b \frac{k^2 V^2}{b^2} + \frac{ikVg}{b} [\omega_h]_b [M_{ii}]_b + [K_{ii}] + q[Q_{hh}(ik)]$$

The determinant of $[C_{hh}(ik)]$ is sometimes called the flutter determinant. It becomes zero when the dynamic pressure q , the true airspeed V and the reduced frequency k are at their flutter boundary values. The values of V and q reflect design flight conditions at which the open-loop system is stable for all the tabulated k_ℓ values. The modal damping g is one of the user-input weighting parameters discussed in Section 3.5.2.

The weights assigned to the terms of a data matrix $[Q_{hh}(ik_\ell)]$ are based on their effect on the determinant of the system matrix $[C_h(ik_\ell)]$ of Eq. (3.31). The absolute values of the partial derivatives of this determinant with respect to $Q_{hh_{ij}}(ik_\ell)$, divided by the determinant itself, is shown in [4] to be the ij -th term of the weight matrix

$$[\bar{W}_{hh}]_\ell = q |[C_{hh}(ik_\ell)]^{-1}|^T \quad (3.32)$$

The weights assigned to the terms in the j -th column of a data matrix $[Q_{hc}(ik_\ell)]$ is based on the open-loop Nyquist frequency response of the j -th actuator to excitation by the j -th control surface. The actuator response is related to the modal response by

$$\{\delta(i\omega)\} = [T(i\omega)][\phi_{sh}]\{\xi(i\omega)\} \quad (3.33)$$

where $[T(i\omega)]$ is a matrix of transfer functions relating actuator outputs to sensor inputs, and $[\phi_{sh}]$ is the matrix of modal deflections at sensor inputs. The physical-weighting transfer functions in $[T(i\omega)]$ should be simple and unrelated to particular aeroservoelastic parameters. Structural, narrow-band filters with high sensitivity to parametric changes should not be included as it may result in the assignment of low weights to important aerodynamic data terms. Hence, the physical weighting algorithm assumes transfer functions which are based on a third-order actuator, multiplied by a control gain. The magnitude of the partial derivative of the Nyquist signal with respect to $Q_{hc,j}(ik_\ell)$ is shown in [4] to be the ij -th term of the weight matrix

$$[\bar{W}_{hc}]_\ell = q \left| [T(ik_\ell)][\phi_{sh}][C_{hh}(ik_\ell)]^{-1} \right|^T \quad (3.34)$$

The weights assigned to the terms of the j -th column of a data matrix $[Q_{hG}(ik_\ell)]$ is based on the power spectral density (PSD) of the open-loop response of a selected structural acceleration to continuous gust, derived from Eq. (3.31),

$$\Phi_{z_j}(k_\ell) = \left| \frac{k_\ell^2 q V}{b^2} [\phi_{zh_j}][C_{hh}(ik_\ell)]^{-1} \{Q_{hG_j}(ik_\ell)\} \right|^2 \Phi_{w_j}(k_\ell) \quad (3.35)$$

where $[\phi_{zh_j}]$ is a row vector of modal displacements at the selected response point, and $\Phi_{w_j}(k)$ is the PSD function of the associated gust velocity,

$$\Phi_{w_j}(k_\ell) = \frac{\sigma_{w_j}^2}{\pi} \frac{L_g}{V} \frac{1 + 3(k_\ell L_g/b)^2}{[1 + (k_\ell L_g/b)^2]^2}$$

where $\sigma_{w_j}^2$ j -th gust RMS velocity, and L_g is the gust characteristic length. The partial derivative of $\sqrt{\Phi_{z_j}(k_\ell)}$ with respect to $Q_{hG_{ij}}(ik_\ell)$ is the ij -th term of the weight matrix

$$[\bar{W}_{hG}]_\ell = \frac{k_\ell^2 q V}{b^2} \left| [\phi_{zh}] [C_{hh}(ik_\ell)]^{-1} \right|^T [\bar{\Phi}_w]_\ell \quad (3.36)$$

where $[\bar{\Phi}_w]_\ell$ in an $n_G \times n_G$ diagonal matrix whose elements are $\sqrt{\Phi_{w_j}(k_\ell)}$.

3.5.2 Weight scaling and modifications

The variations of terms in the weight groups $[\bar{W}_{hh}]_\ell$, Eq. (3.32), $[\bar{W}_{hc}]_\ell$, Eq. (3.34), and $[\bar{W}_{hG}]_\ell$, Eq. (3.36), with k may have very sharp peaks. In addition, the peak values of many terms may be several orders-of-magnitude smaller than other peaks. The extreme weight variations have the effect of neglecting much of the data, which may cause numerical ill-conditioning problems and unrealistic curve fits. To ensure realistic interpolation between the tabulated k values, and to facilitate the application of the resulting aeroelastic model to a variety of flow conditions, structural modifications, and control parameters, it may be desirable to moderate the weight variations. This can be done by one or a combination of the following means:

- assignment of a relatively large damping parameter g in Eq. (3.31),
- widening the weight peaks,
- scaling up the extremely low weights.

Peak widening is performed in n_{wd} cycles applied sequentially to each weights, $\bar{W}_{ij}(k_\ell)$, of the 3 weight groups. In each cycle, $\bar{W}_{ij}(k_\ell)$ is changed to $\max\{\bar{W}_{ij}(k_{\ell-1}), \bar{W}_{ij}(k_\ell), \bar{W}_{ij}(k_{\ell+1})\}$ of the previous cycle. The weight matrices are then normalized and combined to the final weight matrix

$$[W_h]_\ell = \begin{bmatrix} [W_{hh}]_\ell & [W_{hc}]_\ell & [W_{hG}]_\ell \end{bmatrix} \quad (3.37)$$

where a term in $[W_{hh}]_\ell$ is

$$W_{hh_{ij\ell}} = \left(\max \left\{ \frac{1}{\max_{i,j} \{\tilde{W}_{hh_{ij}}\}}, \frac{W_{cut}}{\tilde{W}_{hh_{ij}}} \right\} \right) \bar{W}_{hh_{ij\ell}} \quad (3.38)$$

where

$$\tilde{W}_{hh_{ij}} = \max_{\ell} \left\{ |Q_{hh_{ij}}(ik_{\ell})| \bar{W}_{hh_{ij\ell}} \right\} \quad (3.39)$$

and the terms of $[W_{hc}]_\ell$ and $[W_{hG}]_\ell$ are calculated similarly (but separately). The upscale parameter W_{cut} is defined by the user. The resulting magnitudes of the weighted terms,

$$\bar{Q}_{h_{ij}}(k_{\ell}) = W_{h_{ij\ell}} |Q_{h_{ij}}(ik_{\ell})| \quad (3.40)$$

fall between W_{cut} and 1.0 when the value of 1.0 typically appears only once in each group. The modified physical weighting is actually a compromise between the the unmodified one (with n_{wd} and W_{cut} equal zero) and the data-normalization weighting of Ref. [4]. With $n_{wd} = n_{\ell}$ and $W_{cut} = 1.0$, all the physical-weighting effects are suppressed and the weighting becomes a data-normalization one. Recommended parameters in typical cases [5] are $n_{wd} = 2$ and $W_{cut} = 0.01$. Various applications demonstrated that the resulting aeroservoelastic models were adequate for analyses with large variations of dynamic pressures [4-6, 11], control gains [12], and structural parameters [13].

3.5.3 Relative importance of modes

The physical weights can be used to rate the vibration modes according to their relative aeroelastic importance. Based on the magnitudes of the weighted aerodynamic data terms, Eq. (3.40), calculated with n_{wd} and W_{cut} equal zero, three modal measures of aeroelastic importance are defined for each structural vibration mode by

$$\begin{aligned} Q_{h_i}^* &= \max_{j,\ell} \left\{ |\bar{Q}_{hh_{ij}}(ik_{\ell})| \right\}, & Q_{c_i}^* &= \max_{j,\ell} \left\{ |\bar{Q}_{hc_{ij}}(ik_{\ell})| \right\}, \\ Q_{g_i}^* &= \max_{j,\ell} \left\{ |\bar{Q}_{hG_{ij}}(ik_{\ell})| \right\} \end{aligned} \quad (3.41)$$

These measures can be interpreted as indicators of the aeroelastic activity of the i -th vibration mode, on a scale of 0 to 1, in three categories: a) influence on the open-loop system roots (Q_s^*); b) role in the aeroservoelastic loop (Q_c^*); and c) contribution to gust response (Q_g^*). Being based on a limited analysis, these measures should be used with caution. Their main usage is in supplying physical insight and in pointing out the structural modes that can be eliminated in subsequent analyses from the model without causing significant errors.

Chapter 4

State-Space Aeroservoelastic Equations

The time-domain ASE model for stability analysis is constructed from the separate models of the aeroelastic plant, the sensing and actuation models and the control system, all expressed in state-space. In the aeroelastic model, each modal coordinate is represented by two states: the modal displacement and its velocity. Rational approximation of the unsteady AFC matrices in the Laplace s domain facilitates the augmentation to incorporate the aerodynamic states in the model. The system matrix of the plant model can be used for flutter analysis of the open-loop aeroelastic plant. The control system includes the control surfaces driven by actuators, sensors related to the structural degrees of freedom, and a linear MIMO control law that relates the actuator inputs to the sensor readings. The full ASE model can be used for control margin computation and for closed-loop flutter analyses. Since only stability and flutter issues are addressed in this chapter, no external inputs, such as pilot commands and wind gust inputs, are incorporated in the model.

4.1 Aeroelastic Model

The second-order time-domain equation of motion of the structure was defined in Eq. (2.23), with the generalized external forces represented by $\{P_h(t)\}$. For stability analysis of the

open-loop aeroelastic system or the closed-loop aeroservoelastic system, $\{P_h(t)\}$ includes aerodynamic forces due to structural dynamics, and inertial and aerodynamic forces due to control-surface motion.

The control-induced inertial forces are defined in Eq. (2.28). The generalized aerodynamic forces are defined in the frequency domain in Eq. (2.38). The aerodynamic force coefficient (AFC) matrices are first calculated at several user-defined tabulated reduced frequency values, k_t , similar to a regular frequency domain flutter analysis. The tabulated matrices are used for approximating the AFC matrix as a rational function of k in the entire frequency domain, as described in Chapter 3. An expansion to the entire Laplace domain is performed by replacing ik in the rational expression by the non-dimensional Laplace variable $p = sb/V$, which yields Eq. (3.2). The substitution of $p = sb/V$ in the expression for $[\tilde{Q}_h(p)]$ of Eq. (3.2) gives

$$[\tilde{Q}_h(s)] = [A_{h0}] + \frac{b}{V}[A_{h1}]s + \frac{b^2}{V^2}[A_{h2}]s^2 + [D_h] \left([I]s - \frac{V}{b}[R] \right)^{-1} [E]s \quad (4.1)$$

The $[A_{hi}]$ and $[E]$ matrices are column partitioned as

$$[A_{hn}] = [A_{hhn} \quad A_{hcn}] \quad (n = 0, 1, 2), \quad [E] = [E_h \quad E_c]$$

As stated at the beginning of Chapter 3, the coefficient matrices in Eq. (4.1) are calculated for the baseline structure with the generalized matrices associated with the original modes $[\phi_{ai}]$, before the transformation of Eq. (2.21) is made. The actual modes that serve as generalized coordinates in each optimization iteration are $[\phi_{ah}]$ which relates to $[\phi_{ai}]$ via $[\psi]$ using Eq. (2.22). Consequently, the coefficient matrices of Eq. (4.1) have to be updated in each iteration by

$$[A_{hhn} \quad A_{hcn}] = [\psi]^T [A_{iin} \psi \quad A_{icn}], \quad [D_h] = [\psi]^T [D_i], \quad [E_h] = [E_i][\psi] \quad (4.2)$$

where the subscripts i relate to the matrices calculated in the rational approximation process, denoted in Chapter 3 with subscripts h .

To facilitate state-space formulation, an augmenting aerodynamic state vector of dimension n_a is defined by its Laplace transform as

$$\{x_a(s)\} = \left([I]s - \frac{V}{b}[R] \right)^{-1} ([E_h]\{\xi(s)\} + [E_c]\{\delta_c(s)\}) s \quad (4.3)$$

Equation (3.1) without the gust term and Eqs. (4.1-4.3) yield the s-plane generalized aerodynamic force vector

$$\begin{aligned} \{P_h^a(s)\} &= -q[\tilde{Q}_{hh}(s)]\{\xi(s)\} - q[\tilde{Q}_{hc}(s)]\{\delta_c(s)\} \\ &= -q \left([A_{hh_0}] + \frac{b}{V}[A_{hh_1}]s + \frac{b^2}{V^2}[A_{hh_2}]s^2 \right) \{\xi(s)\} \\ &\quad - q \left([A_{hc_0}] + \frac{b}{V}[A_{hc_1}]s + \frac{b^2}{V^2}[A_{hc_2}]s^2 \right) \{\delta_c(s)\} \\ &\quad - q[D_h]\{x_a(s)\} \end{aligned} \quad (4.4)$$

Equations (2.23), (2.28) and the time-domain version of Eq. (4.4) yield the state-space open-loop aeroelastic equation of motion

$$\{\dot{x}_{ae}\} = [A_{ae}]\{x_{ae}\} + [B_{ae}]\{u_{ae}\} \quad (4.5)$$

where

$$\{x_{ae}\} = \begin{Bmatrix} \xi \\ \dot{\xi} \\ x_a \end{Bmatrix} \quad \{u_{ae}\} = \begin{Bmatrix} \delta_c \\ \dot{\delta}_c \\ \ddot{\delta}_c \end{Bmatrix}$$

$$\begin{aligned} [A_{ae}] &= \begin{bmatrix} 0 & [I] & 0 \\ -[\bar{M}]^{-1}[K_{hh} + qA_{hh_0}] & -[\bar{M}]^{-1}\left[B_{hh} + \frac{qb}{V}A_{hh_1}\right] & -q[\bar{M}]^{-1}[D_h] \\ 0 & [E_h] & \frac{V}{b}[R] \end{bmatrix} \\ [B_{ae}] &= \begin{bmatrix} 0 & 0 & 0 \\ -q[\bar{M}]^{-1}[A_{hc_0}] & -\frac{qb}{V}[\bar{M}]^{-1}[A_{hc_1}] & -[\bar{M}]^{-1}\left[M_{hc} + \frac{qb^2}{V^2}A_{hc_2}\right] \\ 0 & [E_c] & 0 \end{bmatrix} \end{aligned}$$

$$[\bar{M}] = [M_{hh}] + \frac{qb^2}{V^2} [A_{hh_2}]$$

The number of states in Eq. (4.5) is $2n_h + n_a$.

The outputs of the aeroelastic plant are sensor readings. It is assumed here that the sensors measure either structural displacements, velocities or accelerations, and that the measurements are perfect. Sensor dynamics can be modeled in series with the sensors' outputs and incorporated in the ASE model as part of the control system, discussed in the sequel. The outputs are assumed to be linear combinations of the structural state response. The combinations are defined by the modal displacement (or rotation) row vector $[\phi_y]$ at the sensor location. Thus, a displacement sensor reads

$$y_d = \begin{bmatrix} \phi_y & 0 & 0 \end{bmatrix} \{x_{ae}\} \quad (4.6)$$

A velocity (rate) sensor reads

$$y_v = \begin{bmatrix} 0 & \phi_y & 0 \end{bmatrix} \{x_{ae}\} \quad (4.7)$$

and an accelerometer reads

$$\begin{aligned} y_a &= [\phi_y] \{\ddot{\xi}\} \\ &= -[\phi_y][\bar{M}]^{-1} \left(\begin{bmatrix} [K_{hh} + qA_{hh_0}] & [B_{hh} + \frac{qb}{V}A_{hh_1}] & q[D_h] \end{bmatrix} \{x_{ae}\} + \right. \\ &\quad \left. + \begin{bmatrix} q[A_{hc_0}] & \frac{qb}{V}[A_{hc_1}] & [M_{hc} + \frac{qb^2}{V^2}A_{hc_2}] \end{bmatrix} \{u_{ae}\} \right) \end{aligned} \quad (4.8)$$

In general, the output of n_s sensor readings can be expressed by

$$\{y_{ae}\} = [C_{ae}]\{x_{ae}\} + [D_{ae}]\{u_{ae}\} \quad (4.9)$$

4.2 Actuator Model

The dynamic model of the actuator driving the i -th control surface is specified by a transfer function having the form

$$\frac{\delta_{c_i}(s)}{u_{ac_i}(s)} = \frac{a_{i3}}{s^3 + a_{i1}s^2 + a_{i2}s + a_{i3}} \quad (4.10)$$

where u_{ac_i} is the servo-commanded (actuator input) control surface deflection. The DC ($s = 0$) gain of the transfer function in Eq. (4.10) is one, and thus in steady state $u_{ac_i} = \delta_{c_i}$.

The order difference of three between the numerator and denominator in Eq. (4.10) is justified on physical grounds: second order difference represents the control surface deflection response to a force input and a first order lag used to model the realistically limited bandwidth of the actuator. Due to this order difference, δ_i , $\dot{\delta}_i$ and $\ddot{\delta}_i$ can be defined as independent states in the actuator state-space model, and thus used directly as inputs to Eq. (4.5) and in connections to acceleration sensors. Higher order actuator dynamics can be defined by connecting additional transfer functions in series to u_{ac_i} . These additional transfer functions can be included as part of the control system model discussed in the following section.

A state-space realization of the actuator dynamics of Eq. (4.10) is

$$\{\dot{x}_{ac_i}\} = \begin{bmatrix} 0 & 1 & 0 \\ 0 & 0 & 1 \\ -a_{i3} & -a_{i2} & -a_{i1} \end{bmatrix} \{x_{ac_i}\} + \begin{bmatrix} 0 \\ 0 \\ a_{i3} \end{bmatrix} u_{ac_i} \quad (4.11)$$

where

$$\{x_{ac_i}\} = \begin{Bmatrix} \delta_{c_i} \\ \dot{\delta}_{c_i} \\ \ddot{\delta}_{c_i} \end{Bmatrix}$$

For system with $n_c > 1$ actuators, the state-space model of all the actuators is arranged so that the total actuator state vector $\{x_{ac}\}$ equals to the input vector $\{u_{ac}\}$ of Eq. (4.5). Thus the actuator state vector and inputs are

$$\{x_{ac}\} = \begin{Bmatrix} \delta_c \\ \dot{\delta}_c \\ \ddot{\delta}_c \end{Bmatrix} \quad \{u_{ac}\} = \begin{Bmatrix} u_{ac_1} \\ \vdots \\ u_{ac_{n_c}} \end{Bmatrix}$$

where $\{\delta_c\}^T = [\delta_{c_1} \ \delta_{c_2} \ \cdots \ \delta_{c_{n_c}}]$. The state-space equation for $\{x_{ac}\}$ is

$$\{\dot{x}_{ac}\} = \begin{bmatrix} 0_{2n_c \times n_c} & I_{2n_c \times 2n_c} \\ -A_{ac3} & -A_{ac2} & -A_{ac1} \end{bmatrix} \{x_{ac}\} + \begin{bmatrix} 0_{2n_c \times n_c} \\ A_{ac3} \end{bmatrix} \{u_{ac}\} \quad (4.12)$$

where $0_{2n_c \times n_c}$ and $I_{2n_c \times 2n_c}$ are, respectively, zero and identity matrices of appropriate dimensions, and $[A_{ac_i}]$, $i = 1, 2, 3$ are diagonal matrices defined by

$$[A_{ac_i}] = \text{diag}\{a_{1i}, \dots, a_{n_{ci}}\}$$

Equation (4.12) can be stated in a compact form as

$$\{\dot{x}_{ac}\} = [A_{ac}]\{x_{ac}\} + [B_{ac}]\{u_{ac}\} \quad (4.13)$$

Since $\{x_{ac}\} = \{u_{ae}\}$, the augmentation of the aeroelastic states $\{x_{ae}\}$ of Eq. (4.5) to include the actuator states $\{x_{ac}\}$ of Eq. (4.13) yields

$$\{\dot{x}_p\} = [A_p]\{x_p\} + [B_p]\{u_p\} \quad (4.14)$$

where

$$\{x_p\} = \begin{Bmatrix} x_{ae} \\ x_{ac} \end{Bmatrix} \quad [A_p] = \begin{bmatrix} A_{ae} & B_{ae} \\ 0 & A_{ac} \end{bmatrix} \quad [B_p] = \begin{bmatrix} 0 \\ B_{ac} \end{bmatrix}$$

The output (sensor measurement) equation (4.9) becomes

$$\{y_p\} = [C_p]\{x_p\} \quad (4.15)$$

where

$$[C_p] = \begin{bmatrix} C_{ae} & D_{ae} \end{bmatrix}$$

Note that in equation (4.15) there is no direct feed-through between the input $\{u_p\}$ and the output $\{y_p\}$. This results from the limited bandwidth of the actuators.

4.3 Control System Model

The control system is modeled as an interconnection of three types of basic control elements in addition to a variable gain matrix. The interconnections within the control elements and between them and the aeroelastic (AE) system can be either fixed or through the variable

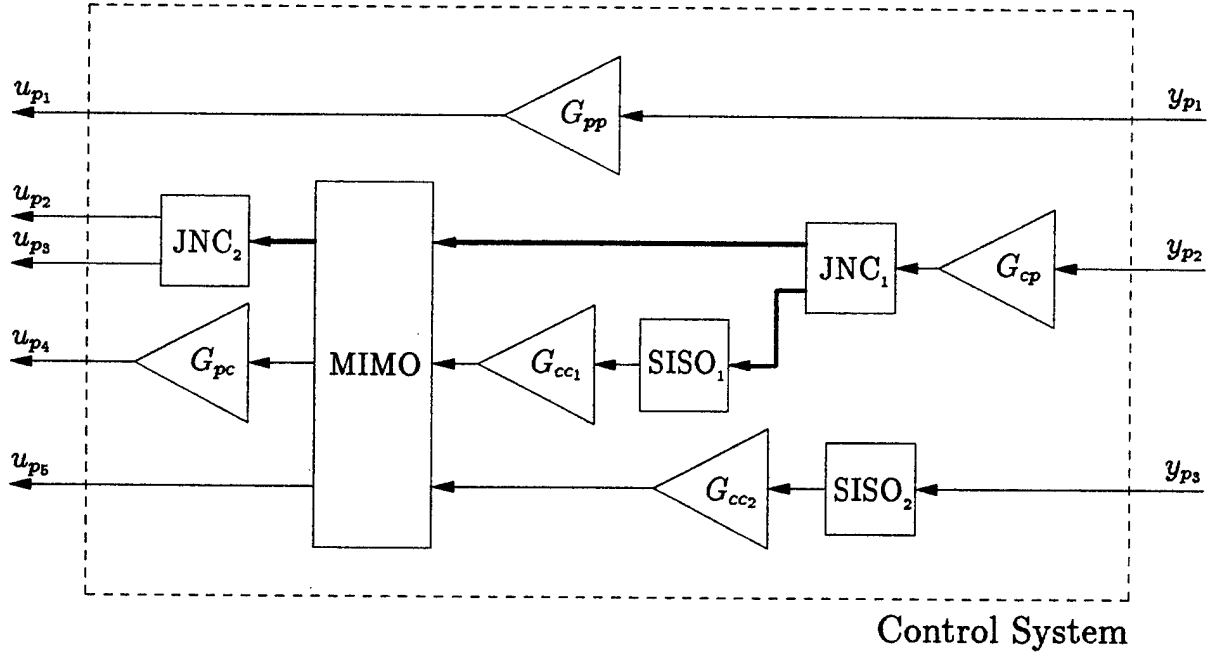


Figure 4.1: The control system interconnection model. Thick lines represent fixed connections. y_{p_i} , $i = 1, 2, 3$ are the sensor reading inputs and u_{p_i} , $i = 1, \dots, 5$ are outputs to the actuators.

gain matrix, the elements of which are subject to subsequent stability margin analysis, as demonstrated schematically in Figure 4.1.

The ASE model can be used for parameter optimization of the AE system. In this optimization process, the control system is assumed to be constant, except of possible variations in the variable gain matrix elements. Thus, only the AE and variable gain matrix are changing in the ASE model during the optimization. To avoid unnecessary recalculation of the *entire* ASE model due to those changes, the control system with the *fixed* connections is constructed only once and is reused in the ASE model reconstruction throughout the optimization process, thus reducing computational load. Clearly, if the control system is updated as a result of significant changes in the AE model, the entire ASE model has to be reconstructed.

4.3.1 Control System Elements

The control system is constructed from three types of elements: single-input-single-output (SISO) elements specified as transfer functions, multi-input-multi-output (MIMO) elements defined in state-space, and zero-order junctions. The parameters of these elements are assumed to be constant. The overall control system variations are accounted in the above mentioned variable gain matrix.

SISO Control Elements

A SISO control element is defined by a proper transfer function $T_{se}(s)$, which is then realized in state-space inside the ASE module. A general transfer function from the input $u_{se,i}$ to the output $y_{se,i}$ is expressed by a ratio of polynomials in s

$$T_{se,i}(s) = \frac{y_{se,i}(s)}{u_{se,i}(s)} = \frac{b_{0,i}s^n + b_{1,i}s^{n-1} + \dots + b_{n,i}}{s^n + a_{1,i}s^{n-1} + \dots + a_{n,i}} \quad (4.16)$$

The controller canonical realization of Eq. (4.16) is

$$\begin{aligned} \{\dot{x}_{se,i}\} &= [A_{se,i}]\{x_{se,i}\} + \{B_{se,i}\}u_{se,i} \\ y_{se,i} &= [C_{se,i}]\{x_{se,i}\} + D_{se,i}u_{se,i} \end{aligned} \quad (4.17)$$

where

$$\begin{aligned} [A_{se,i}] &= \begin{bmatrix} 0 & & & \\ \vdots & I_{(n-1) \times (n-1)} & & \\ 0 & & & \\ -a_{n,i} & -a_{n-1,i} & \dots & -a_{1,i} \end{bmatrix} & \{B_{se,i}\} &= \begin{bmatrix} 0 \\ \vdots \\ 0 \\ 1 \end{bmatrix} \\ [C_{se,i}] &= \begin{bmatrix} (b_{n,i} - b_{0,i}a_{n,i}) & (b_{n-1,i} - b_{0,i}a_{n-1,i}) & \dots & (b_{1,i} - b_{0,i}a_{1,i}) \end{bmatrix} \\ D_{se,i} &= b_{0,i} \end{aligned} \quad (4.18)$$

The number of states in $\{x_{se,i}\}$ is equal to the order n of the denominator polynomial in Eq. (4.16).

MIMO State-Space Control Elements

A MIMO state-space control element is defined by its order (number of states), the number of inputs and outputs, and the associated state space dynamics and output matrices. These matrices are defined by the user as direct matrix input (DMI) entries or by INPUTT2 MAPOL commands. This facilitates interaction with external control design codes. The equations of a MIMO state-space element are

$$\begin{aligned}\{\dot{x}_{me,i}\} &= [A_{me,i}]\{x_{me,i}\} + [B_{me,i}]\{u_{me,i}\} \\ \{y_{me,i}\} &= [C_{me,i}]\{x_{me,i}\} + [D_{me,i}]\{u_{me,i}\}\end{aligned}\tag{4.19}$$

A special case of Eq. (4.19) is a SISO element specified in state-space format, in which case $[B_{me,i}]$ is a column vector, $[C_{me,i}]$ is a row vector and $[D_{me,i}]$ is a scalar.

Zero-Order Control Elements

A zero-order element is defined by its number of inputs and number of outputs. This is a junction element in which every output is a weighted sum of the inputs. The element equation is simply

$$\{y_{je,i}\} = [D_{je,i}]\{u_{je,i}\}\tag{4.20}$$

where the element of $[D_{je,i}]$ are the various weights, which can be positive, negative or zero.

Clearly, the zero-order element is a special case of a MIMO element. It is separately introduced, however, to simplify the input format and internal assembling.

4.3.2 Fixed Connections in the Control System Model

The overall control system is constructed as an interconnection of the above defined control elements and the variable gain matrix, discussed in more detail in the next section. To construct this interconnection, all the control system elements are combined into one (not

connected yet) state-space model

$$\begin{aligned} \begin{Bmatrix} \dot{x}_{se} \\ \dot{x}_{me} \end{Bmatrix} &= \begin{bmatrix} A_{se} & 0 \\ 0 & A_{me} \end{bmatrix} \begin{Bmatrix} x_{se} \\ x_{me} \end{Bmatrix} + \begin{bmatrix} B_{se} & 0 & 0 \\ 0 & B_{me} & 0 \end{bmatrix} \begin{Bmatrix} u_{se} \\ u_{me} \\ u_{je} \end{Bmatrix} \\ \begin{Bmatrix} y_{se} \\ y_{me} \\ y_{je} \end{Bmatrix} &= \begin{bmatrix} C_{se} & 0 \\ 0 & C_{me} \\ 0 & 0 \end{bmatrix} \begin{Bmatrix} x_{se} \\ x_{me} \end{Bmatrix} + \begin{bmatrix} D_{se} & 0 & 0 \\ 0 & D_{me} & 0 \\ 0 & 0 & D_{je} \end{bmatrix} \begin{Bmatrix} u_{se} \\ u_{me} \\ u_{je} \end{Bmatrix} \end{aligned} \quad (4.21)$$

where the various blocks represent all the elements of the same type. For each block, its state, input and output vectors combine all the element vectors, and the state-space matrices are block diagonal. As an example, the SISO elements are grouped as follows:

$$\{x_{se}\} = \begin{Bmatrix} x_{se,1} \\ \vdots \\ x_{se,n_{se}} \end{Bmatrix} \quad \{u_{se}\} = \begin{Bmatrix} u_{se,1} \\ \vdots \\ u_{se,n_{se}} \end{Bmatrix} \quad \{y_{se}\} = \begin{Bmatrix} y_{se,1} \\ \vdots \\ y_{se,n_{se}} \end{Bmatrix}$$

$$\begin{aligned} [A_{se}] &= \text{diag} [A_{se,1} \cdots A_{se,n_{se}}] & [B_{se}] &= \text{diag} [B_{se,1} \cdots B_{se,n_{se}}] \\ [C_{se}] &= \text{diag} [C_{se,1} \cdots C_{se,n_{se}}] & [D_{se}] &= \text{diag} [D_{se,1} \cdots D_{se,n_{se}}] \end{aligned}$$

where n_{se} is the number of SISO elements. The same construction is performed for the n_{me} MIMO and the n_{je} zero-order elements.

For simplicity, it is assumed that the input and output of a fixed connections cannot appear in another connection. Thus, if an output of an element is used as an input to more than one other element, it should be first connected to a "splitting" zero-order junction with unity weights, the outputs of which can then be used as necessary. Similarly, if an input of an element is a sum of outputs of several other elements, it should be preceded with a summing junction (many inputs and one output). To avoid confusion, an output of a control element *cannot* be connected to its own input. After the fixed connections are applied, the associated inputs and output are eliminated from the equations of motion.

In a fixed connection among control elements, an input of a control element u_{e_i} is set equal to an output of another control element y_{e_j} , namely $u_{e_i} = y_{e_j}$. To perform all these

connections, we rewrite the state-space model of Eq. (4.21) and re-arrange its inputs and outputs as follows:

$$\begin{aligned} \begin{Bmatrix} \dot{x}_e \end{Bmatrix} &= \begin{bmatrix} A_e \end{bmatrix} \begin{Bmatrix} x_e \end{Bmatrix} + \begin{bmatrix} B_{e_1} & B_{e_2} \end{bmatrix} \begin{Bmatrix} u_{e_1} \\ u_{e_2} \end{Bmatrix} \\ \begin{Bmatrix} y_{e_1} \\ y_{e_2} \end{Bmatrix} &= \begin{bmatrix} C_{e_1} \\ C_{e_2} \end{bmatrix} \begin{Bmatrix} x_e \end{Bmatrix} + \begin{bmatrix} D_{e_{11}} & D_{e_{12}} \\ D_{e_{21}} & D_{e_{22}} \end{bmatrix} \begin{Bmatrix} u_{e_1} \\ u_{e_2} \end{Bmatrix} \end{aligned} \quad (4.22)$$

where $\{u_{e_2}\}$ and $\{y_{e_2}\}$ are the inputs and outputs which are involved in fixed connections. Obviously, the dimensions of $\{u_{e_2}\}$ and $\{y_{e_2}\}$ are equal. The assumption that u_{e_i} and y_{e_j} of a certain fixed connection cannot appear in another connection implies that

$$\{u_{e_2}\} = [I_2]\{y_{e_2}\} \quad (4.23)$$

where $[I_2]$ is square matrix with ones at the (i, j) connection entries and zero elsewhere, i.e., each row or column of $[I_2]$ has only one non-zero entry set to one. Substituting Eq. (4.23) in Eq. (4.22) yields the control system equation

$$\begin{aligned} \{\dot{x}_c\} &= [A_c]\{x_c\} + [B_c]\{u_c\} \\ \{y_c\} &= [C_c]\{x_c\} + [D_c]\{u_c\} \end{aligned} \quad (4.24)$$

where $\{x_c\} = \{x_e\}$, $\{u_c\} = \{u_{e_1}\}$, $\{y_c\} = \{y_{e_1}\}$, and

$$\begin{aligned} [A_c] &= [A_e] + [B_{e_2}][I_2][\tilde{C}_{e_2}] \\ [B_c] &= [B_{e_1}] + [B_{e_2}][I_2][\tilde{D}_{e_{21}}] \\ [C_c] &= [C_{e_1}] + [D_{e_{12}}][I_2][\tilde{C}_{e_2}] \\ [D_c] &= [D_{e_{11}}] + [D_{e_{12}}][I_2][\tilde{D}_{e_{21}}] \\ \begin{bmatrix} \tilde{C}_{e_2} \\ \tilde{D}_{e_{21}} \\ \tilde{D}_{e_{22}} \end{bmatrix} &= \begin{bmatrix} \tilde{D}_{e_{22}}[C_{e_2}] \\ \tilde{D}_{e_{22}}[D_{e_{21}}] \\ [I - D_{e_{22}}I_2]^{-1} \end{bmatrix} \end{aligned} \quad (4.25)$$

The well-posedness of the connections in Eq. (4.23) guarantees that $[I - D_{e_{22}}I_2]^{-1}$ exists.

The model structure and its parameters/matrixes in Eqs. (4.24) and (4.25) are independent of the structural and aerodynamic variables and thus are unchanged in the design or optimization process of the latter

4.4 The ASE Model

The ASE model is obtained by connecting the AE model of Eqs. (4.14) and (4.15) with the control system of Eq. (4.24) through fixed and variable gain connections, as shown schematically in Figure 4.2. As in subsection 4.3.2, an input and output of one fixed connection cannot appear in another connection.

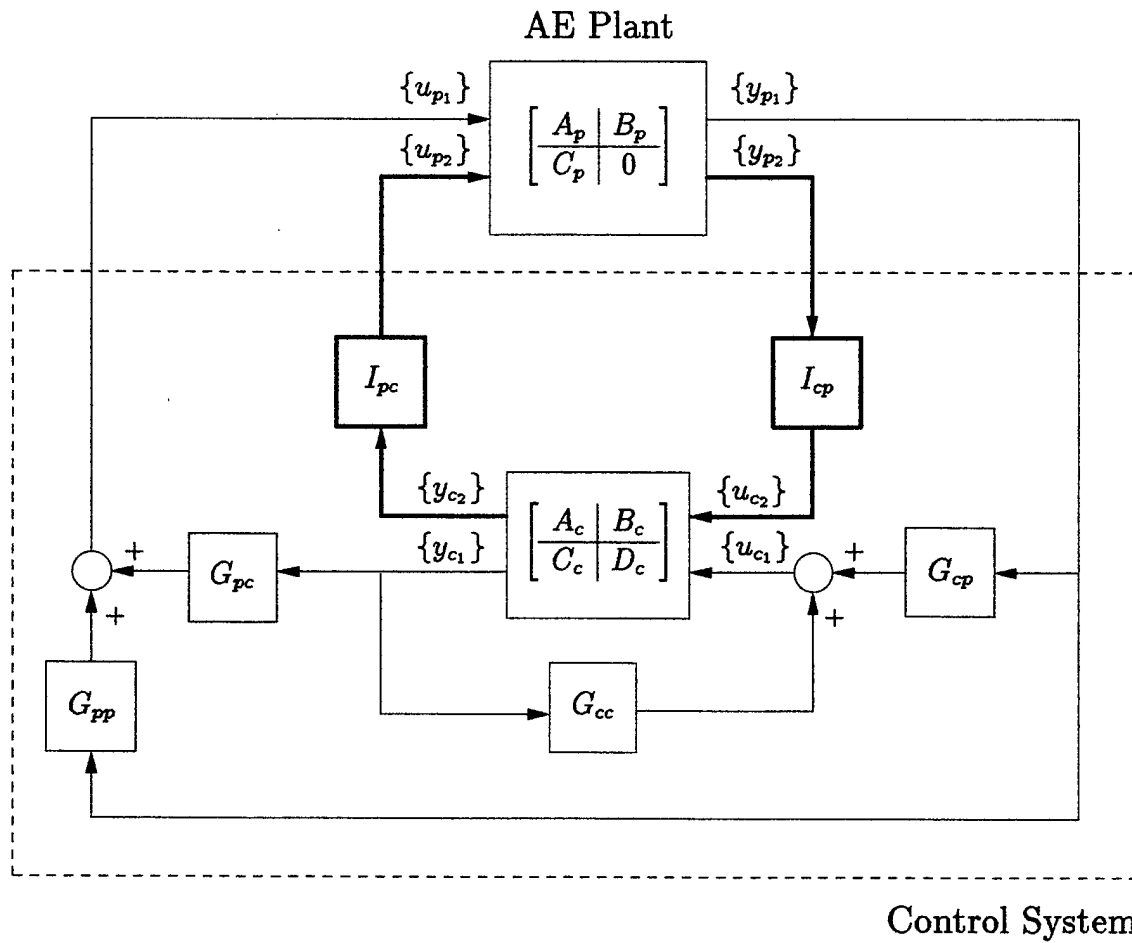


Figure 4.2: The ASE interconnection model. Thick lines represent fixed connections.

To perform these interconnections, the system equations (4.14), (4.15) and (4.24) are assembled and their inputs and outputs are re-arranged as follows:

$$\begin{aligned} \begin{Bmatrix} \dot{x}_p \\ \dot{x}_c \end{Bmatrix} &= \begin{bmatrix} A_p & 0 \\ 0 & A_c \end{bmatrix} \begin{Bmatrix} x_p \\ x_c \end{Bmatrix} + \begin{bmatrix} B_{p1} & B_{p2} & 0 & 0 \\ 0 & 0 & B_{c1} & B_{c2} \end{bmatrix} \begin{Bmatrix} u_{p1} \\ u_{p2} \\ u_{c1} \\ u_{c2} \end{Bmatrix} \\ \begin{Bmatrix} y_{p1} \\ y_{p2} \\ y_{c1} \\ y_{c2} \end{Bmatrix} &= \begin{bmatrix} C_{p1} & 0 \\ C_{p2} & 0 \\ 0 & C_{c1} \\ 0 & C_{c2} \end{bmatrix} \begin{Bmatrix} x_p \\ x_c \end{Bmatrix} + \begin{bmatrix} 0 & 0 & 0 & 0 \\ 0 & 0 & 0 & 0 \\ 0 & 0 & D_{c11} & D_{c12} \\ 0 & 0 & D_{c21} & D_{c22} \end{bmatrix} \begin{Bmatrix} u_{p1} \\ u_{p2} \\ u_{c1} \\ u_{c2} \end{Bmatrix} \end{aligned} \quad (4.26)$$

where inputs and outputs with the subscript 1 are used in connection through the variable gain matrix, while the inputs and outputs with the subscript 2 are used in the fixed connections, performed first. The system with fixed connections closed but variable gain connections open will be referred to as the *gain-open* system.

The fixed connections are specified by

$$\begin{Bmatrix} u_{p2} \\ u_{c2} \end{Bmatrix} = \begin{bmatrix} 0 & I_{pc} \\ I_{cp} & 0 \end{bmatrix} \begin{Bmatrix} y_{p2} \\ y_{c2} \end{Bmatrix} \quad (4.27)$$

where $[I_{pc}]$ and $[I_{cp}]$ are of a similar structure as $[I_2]$ of Eq. (4.23). Eq. (4.27) expresses fixed connections between the AE and control model. Such connections within the control model were already implemented in Eq. (4.24), while fixed connections within the AE model are not logical and thus forbidden. (Any connections from the sensors to actuators are assumed to be part of the control system and thus performed through the elements of the latter.)

Substituting Eq. (4.27) in Eq. (4.26) yields the gain-open vehicle equations

$$\begin{aligned} \{\dot{x}_v\} &= [A_v]\{x_v\} + [B_v]\{u_v\} \\ \{y_v\} &= [C_v]\{x_v\} + [D_v]\{u_v\} \end{aligned} \quad (4.28)$$

where

$$\{x_v\} = \begin{Bmatrix} x_p \\ x_c \end{Bmatrix} \quad \{u_v\} = \begin{Bmatrix} u_{p1} \\ u_{c1} \end{Bmatrix} \quad \{y_v\} = \begin{Bmatrix} y_{p1} \\ y_{c1} \end{Bmatrix}$$

and

$$\begin{aligned} [A_v] &= \begin{bmatrix} A_p + B_{p2} I_{pc} D_{c22} I_{cp} C_{p2} & B_{p2} I_{pc} C_{c2} \\ B_{c2} I_{cp} C_{p2} & A_c \end{bmatrix} & [B_v] &= \begin{bmatrix} B_{p1} & B_{p2} I_{pc} D_{c21} \\ 0 & B_{c1} \end{bmatrix} \\ [C_v] &= \begin{bmatrix} C_{p1} & 0 \\ D_{c12} I_{cp} C_{p2} & C_{c1} \end{bmatrix} & [D_v] &= \begin{bmatrix} 0 & 0 \\ 0 & D_{c11} \end{bmatrix} \end{aligned} \quad (4.29)$$

It can be observed that in Eq. (4.29), direct input-to-output feed-through, i.e., non-zero entries in $[D_v]$, can exist only between u_{c1} and y_{c1} , namely $[D_{c11}]$ connecting between internal control elements. This result is due to the zero feed-through of the AE system discussed in section 4.2, Eq. (4.15).

The final ASE variable gain loop is closed by relating the input vector $\{u_v\}$ to the output vector $\{y_v\}$ via a gain matrix $[G_v]$,

$$\{u_v\} = [G_v]\{y_v\} \quad (4.30)$$

or more specifically

$$\begin{Bmatrix} u_{p1} \\ u_{c1} \end{Bmatrix} = \begin{bmatrix} G_{pp} & G_{pc} \\ G_{cp} & G_{cc} \end{bmatrix} \begin{Bmatrix} y_{p1} \\ y_{c1} \end{Bmatrix} \quad (4.31)$$

G_{pp} represents a direct connection through a variable gain from AE system sensors and actuators, while G_{cc} are control system internal variable gains. G_{cp} and G_{pc} are variable gains specified on the inputs and outputs, respectively, of the control system, i.e., gains on the sensors and to the actuators.

Substituting Eq. (4.30) into Eq. (4.29) yields the closed-loop ASE equations of motion

$$\{\dot{x}_v\} = [\bar{A}_v]\{x_v\} \quad (4.32)$$

where

$$[\bar{A}_v] = [A_v] + [B_v][G_v][I - D_v G_v]^{-1} [C_v] \quad (4.33)$$

The inverse in Eq. (4.33) exists assuming the feedback given by Eq. (4.30) is well posed.

The special structure of the coefficient matrices in Eq. (4.29) is used to reduce the computational load in constructing $[\bar{A}_v]$. In addition, in AE optimization, only elements of the

AE model, i.e., matrices with the subscript p in Eq. (4.29), have to be recomputed, while the rest of the terms in the $[A_v]$, $[B_v]$, $[C_v]$ and $[D_v]$ matrices are unchanged. This can also reduce the computational load in the optimization process.

4.5 System Matrix Derivatives

The derivative of $[\bar{A}_v]$ in Eq. (4.33) with respect to a structural design variable v_i is

$$\frac{\partial[\bar{A}_v]}{\partial v_i} = \frac{\partial[A_v]}{\partial v_i} + [B_v][G_v][I - D_v G_v]^{-1} \frac{\partial[C_v]}{\partial v_i} \quad (4.34)$$

The only terms in $[A_v]$ which are functions of the structural design variables are in $[A_p^{(2)}]$ which combines the second row partitions of $[A_{ae}]$ and $[B_{ae}]$ of Eq. (4.5), namely

$$[A_p^{(2)}] = -[\bar{M}]^{-1}[\tilde{A}_p^{(2)}] \quad (4.35)$$

where

$$[\tilde{A}_p^{(2)}] = \begin{bmatrix} K_{hh} + qA_{hh_0} & B_{hh} + \frac{qb}{V}A_{hh_1} & qD_h & qA_{hc_0} & \frac{qb}{V}A_{hc_1} & \frac{qb^2}{V^2}A_{hc_2} \end{bmatrix}$$

The derivative of $[A_p^{(2)}]$ with respect to v_i is

$$\frac{\partial[A_p^{(2)}]}{\partial v_i} = -[\bar{M}]^{-1} \left([\text{DGMV}]_i [A_p^{(2)}] + \begin{bmatrix} [\text{DGKV}]_i & 0 & 0 & 0 & 0 & [\text{DGMVC}]_i \end{bmatrix} \right) \quad (4.36)$$

where $[\text{DGMV}]_i$, $[\text{DGKV}]_i$ and $[\text{DGMVC}]_i$ are defined in Eqs. (2.7), (2.9), and (2.13), and where use is made of the differentiation formula

$$\frac{\partial[\bar{M}]^{-1}}{\partial v_i} = -[\bar{M}]^{-1} \frac{\partial[\bar{M}]}{\partial v_i} [\bar{M}]^{-1} \quad (4.37)$$

The derivative of $[A_v]$ with respect to v_i is all zero except for the first $2n_h + n_a$ columns in rows $n_h + 1$ to $2n_h$ which are given by Eq. (4.36).

The derivative of $[C_v]$ with respect to v_i is zero in the cases of displacement and velocity measurements. In the case of acceleration measurements, Eq. (4.8) yields

$$\frac{\partial[C_v]}{\partial v_i} = \begin{bmatrix} I & 0 \\ 0 & D_{c_{12}} I_{cp} \end{bmatrix} [\phi_v] \begin{bmatrix} \frac{\partial[A_p^{(2)}]}{\partial v_i} & 0 \end{bmatrix} \quad (4.38)$$

4.6 Aeroelastic System Gain and Its Sensitivities

The aeroelastic system gain is useful in specifying the closed loop ASE system performance. In particular, the zero-frequency (DC) gain of the AE system excluding the rigid body modes, often referred to as the actuator effectiveness, can be used to specify low-frequency performance. Using Eqs. (4.14) and (4.15), the actuator effectiveness is computed by

$$[G_p(0)] = -[C_p][A_p]^{-1}[B_p] \quad (4.39)$$

Its sensitivity with respect to a structural design variable v_i is

$$\frac{\partial[G_p(0)]}{\partial v_i} = \left[[C_p][A_p]^{-1} \frac{\partial[A_p]}{\partial v_i} - \frac{\partial[C_p]}{\partial v_i} \right] [A_p]^{-1}[B_p] \quad (4.40)$$

where the sensitivity matrices $\partial[A_p]/\partial v_i$ and $\partial[C_p]/\partial v_i$ were discussed in the previous section.

Chapter 5

Flutter Analysis

5.1 Flutter Constraints

The flutter analysis is based on the n_{root} eigenvalues λ_l , whose $\text{Im}(\lambda_l) > 0$, of the closed-loop system matrix $[\bar{A}_v]$ of Eq. (4.33). Without a control system, $[\bar{A}_v] \equiv [A_{ae}]$ where $[A_{ae}]$ is the open-loop system matrix defined in Eq. (4.5).

The flutter constraints are those specified in the standard FLUTTER discipline in AS-TROS, namely

$$g = \frac{\gamma_{jl} - \gamma_{jREQ}}{\text{GFACT}} \leq 0 \quad \begin{array}{l} j = 1, 2, \dots, nv \\ l = 1, 2, \dots, n_{root} \end{array} \quad (5.1)$$

where

$$\gamma_{jl} = \frac{\text{Re}(\lambda_l)}{\text{Im}(\lambda_l)}$$

at the j th user-defined velocity associated with a Mach-density pair. The derivative of the flutter constraint with respect to a design variable v_i is

$$\frac{\partial g}{\partial v_i} = \frac{1}{\text{GFACT}} \frac{\partial \gamma_{jl}}{\partial v_i} = \frac{\text{DRRV}_i - \gamma_{jl} \text{DIRV}_i}{\text{Im}(\lambda_l) \text{GFACT}} \quad (5.2)$$

where DRRV_i and DIRV_i are the derivatives of the real and imaginary parts of $\partial \lambda_l / \partial v_i$. Derivatives are calculated for a small portion of the extracted eigenvalues which are the most critical. The computation of $\partial \lambda_l / \partial v_i$ requires the extraction of the eigenvectors associated with λ_l .

5.2 Eigenvalue Sensitivity

The complex column (left) eigenvector $\{X_I\}$ and row (right) eigenvector $\{\bar{X}_I\}^T$ associated with λ_I satisfy

$$([\bar{A}_v] - \lambda_I[I]) \{X_I\} = \{0\} \quad (5.3)$$

and

$$\{\bar{X}_I\}^T ([\bar{A}_v(q_f)] - \lambda_I[I]) = \{0\}^T \quad (5.4)$$

To compute the flutter column eigenvector efficiently, Eq. (5.3) is partitioned into

$$\left(\begin{bmatrix} 0 & I & 0 \\ \bar{A}_{21} & \bar{A}_{22} & \bar{A}_{23} \\ \bar{A}_{31} & \bar{A}_{32} & \bar{A}_{33} \end{bmatrix} - \lambda_I[I] \right) \begin{Bmatrix} X_1 \\ X_2 \\ X_3 \end{Bmatrix} = \{0\} \quad (5.5)$$

where subscript 1 relates to the structural displacement states $\{\xi\}$, 2 relates to the velocity states $\{\dot{\xi}\}$, and 3 relates to the remaining states. The first row partition in Eq. (5.5) yields

$$\{X_1\} = \frac{1}{\lambda_I} \{X_2\} \quad (5.6)$$

which, when substituted in the remaining parts of Eq. (5.5), yields

$$\left(\begin{bmatrix} \bar{A}_{22} + \frac{1}{\lambda_I} \bar{A}_{21} & \bar{A}_{23} \\ \bar{A}_{32} + \frac{1}{\lambda_I} \bar{A}_{31} & \bar{A}_{33} \end{bmatrix} - \lambda_I[I] \right) \begin{Bmatrix} X_2 \\ X_3 \end{Bmatrix} = \{0\} \quad (5.7)$$

The first term in $\{X_2\}$ is set to

$$X_{2_1} = (1.0, 0.0) \quad (5.8)$$

The other values of $\{X_2\}$ and $\{X_3\}$, combined in $\{\tilde{X}\}$, are found by solving

$$([\tilde{A}] - \lambda_I[I]) \{\tilde{X}\} = -\{\tilde{b}\} \quad (5.9)$$

where $[\tilde{A}]$ is the partitioned matrix in the right side of Eq. (5.7), without the first row and first column, and $\{\tilde{b}\}$ is the first column of the partitioned matrix (without the first term).

Eq. (5.9) is solved by first decomposing $[\tilde{A}] - \lambda_I[I]$ into

$$[\tilde{A}] - \lambda_I[I] = [\tilde{L}][\tilde{U}] \quad (5.10)$$

where $[\tilde{L}]$ and $[\tilde{U}]$ are lower and upper triangular matrices. Forward-backward substitution is then performed to yield $\{\tilde{X}\}$, which combines with Eqs. (5.6) and (5.8) to the column eigenvector $\{X_l\}$.

For the computation of the flutter row eigenvector, Eq. (5.4) is partitioned into

$$\begin{Bmatrix} \bar{X}_1 \\ \bar{X}_2 \\ \bar{X}_3 \end{Bmatrix}^T \left(\begin{bmatrix} 0 & I & 0 \\ \bar{A}_{21} & \bar{A}_{22} & \bar{A}_{23} \\ \bar{A}_{31} & \bar{A}_{32} & \bar{A}_{33} \end{bmatrix} - \lambda_l [I] \right) = \{0\}^T \quad (5.11)$$

The first column partition of Eq. (5.11) yields

$$\{\bar{X}_1\} = \frac{1}{\lambda_l} \left([A_{21}]^T \{\bar{X}_2\} + [A_{31}]^T \{\bar{X}_3\} \right) \quad (5.12)$$

which, when substituted in the remaining parts of Eq. (5.11), yields

$$\begin{Bmatrix} \bar{X}_2 \\ \bar{X}_3 \end{Bmatrix}^T \left(\begin{bmatrix} \bar{A}_{22} + \frac{1}{\lambda_l} \bar{A}_{21} & \bar{A}_{23} \\ \bar{A}_{32} + \frac{1}{\lambda_l} \bar{A}_{31} & \bar{A}_{33} \end{bmatrix} - \lambda_l [I] \right) = \{0\} \quad (5.13)$$

Similarly to the column-eigenvector solution, The first term in $\{\bar{X}_2\}$ is set to

$$\bar{X}_{2,1} = (1.0, 0.0) \quad (5.14)$$

and the other values of $\{\bar{X}_2\}$ and $\{\bar{X}_3\}$, combined in $\{\tilde{X}\}$, can now be found by solving

$$\{\tilde{X}\}^T ([\tilde{A}] - \lambda_l [I]) = -\{\tilde{b}\}^T \quad (5.15)$$

where the left-side coefficient matrix is identical to that of Eq. (5.9) but $\{\tilde{b}\}$ now contains the first row of the partitioned matrix, without the first term. In order to solve Eq. (5.15) with the same decomposition used for solving Eq. (5.9), the problem is posed as the conjugate transpose of Eq. (5.15),

$$([\tilde{A}^*] - \lambda_l^* [I])^T \{\tilde{X}^*\} = -\{\tilde{b}^*\} \quad (5.16)$$

from which $\{\tilde{X}\}$ and then the other parts of $\{\bar{X}_l\}$ in Eqs. (5.12) and (5.14) are recovered.

The differentiation of Eq. (5.3) with respect to a design variable v_i yields

$$\left(\frac{\partial [\bar{A}_v]}{\partial v_i} - \frac{\partial \lambda_l}{\partial v_i} [I] \right) \{X_l\} + ([\bar{A}_v] - \lambda_l [I]) \frac{\partial \{X_l\}}{\partial v_i} = \{0\} \quad (5.17)$$

Premultiplication of Eq. (5.17) by $\{\bar{X}_l\}^T$ and the use of Eq. (5.4) yield

$$\frac{\partial \lambda_l}{\partial v_i} \equiv \text{DRRV}_i + i\text{DIRV}_i = \frac{\{\bar{X}_l\}^T \frac{\partial [\bar{A}_v]}{\partial v_i} \{X_l\}}{\{\bar{X}_l\}^T \{X_l\}} \quad (5.18)$$

5.3 Flutter Boundary

While the optimization flutter constraints are based on the system eigenvalues at user-defined flight conditions, the final analysis may include the computation of the flutter velocity at which a root branch crosses to the right side of the Laplace domain. In addition to the n_{vel} major velocity values (V) defined by the user for each Mach-density case, the user defines intermediate V values by specifying the number of equal intervals (n_{dev}) between two consecutive major V values. Starting with the third V value in each Mach-density case, the flutter velocity is calculated when a real part of a complex eigenvalue becomes positive. The total number of V values for which roots are calculated in the final analysis is $nvxn_{dev} + 1$. The k th intermediate V between the major V_m and V_{m+1} is

$$V_k = V_m + \frac{V_{m+1} - V_m}{n_{dev}}(k - 1) \quad (5.19)$$

The flutter velocity and frequency, V_f and ω_f are calculated by quadratic interpolation of the first eigenvalue that crosses to the right side, and the associated ones in the two previous V points. The eigenvalues that correspond to the same "branch" may not appear in the same location in the vectors of eigenvalues associated with different V 's. If, for example, $\lambda_{k,i}$ is the i th eigenvalue in the vector of eigenvalues $\{\lambda\}_k$ associated with V_k , $\lambda_{(k-1),i}$ may not relate to the same aeroelastic branch. It is assumed, however, that the V increments are small such that, the same-branch eigenvalue is the closest one among $\lambda_{(k-1),(i-2)}$ to $\lambda_{(k-1),(i+2)}$. The flutter boundary routine finds the first eigenvalue in each branch (if any), $z_k + i\omega_k$, that has positive real part, and the two previous same-branch eigenvectors, $z_{k-1} + i\omega_{k-1}$ and

$z_{k-2} + i\omega_{k-2}$. The two quadratic interpolation formula are

$$\begin{aligned} V &= V_f + A_q z + B_q z^2 \\ \omega &= \omega_f + A_\omega z + B_\omega z^2 \end{aligned} \quad (5.20)$$

yield the Vandermonde equations

$$\begin{bmatrix} 1 & z_{k-2} & z_{k-2}^2 \\ 1 & z_{k-1} & z_{k-1}^2 \\ 1 & z_k & z_k^2 \end{bmatrix} \begin{Bmatrix} V_f \\ A_q \\ B_q \end{Bmatrix} = \begin{Bmatrix} V_{k-2} \\ V_{k-1} \\ V_k \end{Bmatrix} \quad (5.21)$$

and

$$\begin{bmatrix} 1 & z_{k-2} & z_{k-2}^2 \\ 1 & z_{k-1} & z_{k-1}^2 \\ 1 & z_k & z_k^2 \end{bmatrix} \begin{Bmatrix} \omega_f \\ A_\omega \\ B_\omega \end{Bmatrix} = \begin{Bmatrix} \omega_{k-2} \\ \omega_{k-1} \\ \omega_k \end{Bmatrix} \quad (5.22)$$

which yield

$$V_f = \frac{V_{k-2}z_{k-1}z_k(z_k - z_{k-1}) - V_{k-1}z_{k-2}z_k(z_k - z_{k-2}) + V_k z_{k-2}z_{k-1}(z_{k-1} - z_{k-2})}{(z_k - z_{k-1})(z_k - z_{k-2})(z_{k-1} - z_{k-2})} \quad (5.23)$$

and

$$\omega_f = \frac{\omega_{k-2}z_{k-1}z_k(z_k - z_{k-1}) - \omega_{k-1}z_{k-2}z_k(z_k - z_{k-2}) + \omega_k z_{k-2}z_{k-1}(z_{k-1} - z_{k-2})}{(z_k - z_{k-1})(z_k - z_{k-2})(z_{k-1} - z_{k-2})} \quad (5.24)$$

Chapter 6

Control Stability Margins

This Chapter discusses the controller stability margins of the closed loop ASE system described in Chapter 4. The analysis assumes variations in the gain matrix $[G_v]$ of Eq. (4.30) only, applying both Single-Input-Single-Output (SISO) and Multi-Input-Multi-Output (MIMO) techniques. The SISO stability margin discussions address the single gain uncertainty cases. This includes descriptions of methods to calculate the appropriate SISO transfer functions from the MIMO control system, as well as methods to calculate SISO gain and phase margins and their sensitivities with respect to variations in structural design variables. The SISO techniques are then further extended to treat MIMO problems, where several controller gains can vary simultaneously.

6.1 SISO Stability Margins

The SISO analysis addresses the case of uncertainties or possible variations in one element of the controller gain matrix $[G_v]$, e.g., $G_{v,i,j}$, which takes the form

$$G_{v,i,j} = \bar{G}_{v,i,j} g_{i,j} e^{j\phi_{i,j}} \quad (6.1)$$

Here, $\bar{G}_{v,i,j}$ is the nominal values of $G_{v,i,j}$, while $g_{i,j}$ and $\phi_{i,j}$ are its gain and phase variations, respectively, which determine the gain and phase margins. Their nominal values are $g_{i,j} = 1$ and $\phi_{i,j} = 0$. Assuming that nominally the closed loop ASE system is asymptotically stable,

i.e., $[\bar{A}_v]$ of Eq. (4.33) is Hurwitz with the nominal $\bar{G}_{v,i,j}$, SISO stability margins determine the smallest variations in $g_{i,j}$ and $\phi_{i,j}$ that cause instability of the closed loop ASE system. To compute these margins, appropriate SISO transfer functions have to be constructed from the (generally) MIMO control system. Consequently, the SISO gain and phase margins and their sensitivities to structural design variables can be computed.

6.1.1 SISO Transfer Functions from a MIMO Control System

Computation of the SISO stability margins against variations in $G_{v,i,j}$ discussed above can be efficiently performed by opening the i - j loop of the MIMO control loop in Eq. (4.30) at either input or output side of the gain element $G_{v,i,j}$, resulting in a new single variable input and a new single variable output to the system. The SISO stability margins can then be computed from the open loop SISO transfer function between this new input and the new output.

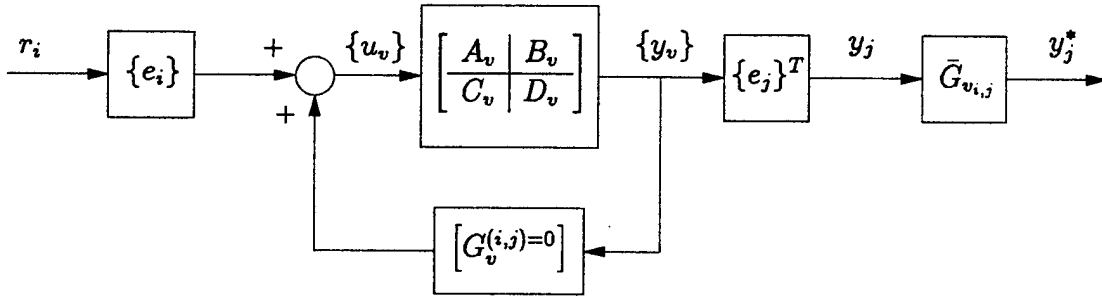


Figure 6.1: SISO stability margins: control loop layout for the required SISO transfer function.

This new SISO transfer function is computed using the “open-closed” loop system depicted schematically in Figure 6.1, where the elements of the new gain matrix $[G_v^{(i,j)=0}]$ are equal to the elements of the nominal gain matrix $[G_v]$, except for the (i,j) element which is set to zero and $\{e_i\}$ and $\{e_j^T\}$ are the i -th and the j -th unit vectors. r_i is the new “external” scalar input and y_j is the new input of this open-closed system.

The MIMO loop in Fig. 6.1 is defined by

$$\{u_v\} = [G_v^{(i,j)=0}] \{y_v\} + \{e_i\} r_i \quad (6.2)$$

Substituting the controller Eq. (6.2) into the system Eq. (4.28), and using the relation

$$y_j^* = \bar{G}_{v,i,j} \{e_j\}^T \{y_v\} \quad (6.3)$$

yields the new open-closed loop system state-space equations

$$\begin{aligned} \{\dot{x}_{oc}\} &= [A_{oc}] \{x_{oc}\} + \{b_{oc,i}\} r_i \\ y_j^* &= [c_{oc,j}] \{x_{oc}\} + d_{oc,j,i} r_i \end{aligned} \quad (6.4)$$

where

$$\begin{aligned} [A_{oc}] &= [A_v] + [\tilde{B}_v] [\tilde{C}_v] \\ \{b_{oc,i}\} &= [B_v] \{e_i\} + [\tilde{B}_v] \{\tilde{D}_{v,i}\} \\ [c_{oc,j}] &= \bar{G}_{v,i,j} \{e_j\}^T [\tilde{C}_v] \\ d_{oc,j,i} &= \bar{G}_{v,i,j} \{e_j\}^T \{\tilde{D}_{v,i}\} \\ [\tilde{B}_v] &= [B_v] [G_v^{(i,j)=0}] \\ [\tilde{C}_v] &= [\bar{D}_v]^{-1} [C_v] \\ \{\tilde{D}_{v,i}\} &= [\bar{D}_v]^{-1} [D_v] \{e_i\} \\ [\bar{D}_v] &= [I - [D_v] [G_v^{(i,j)=0}]] \end{aligned} \quad (6.5)$$

The SISO transfer function between r_i and y_j^* is

$$y_j^*(s) = T_{oc,j,i}(s) r_i(s) \quad (6.6)$$

$$T_{oc,j,i}(s) = [c_{oc,j}] [sI - [A_{oc}]]^{-1} \{b_{oc,i}\} + d_{oc,j,i} \quad (6.7)$$

This transfer function is used next to compute the gain and phase margins of the $\bar{G}_{v,i,j}$ control system gain, and their corresponding sensitivities to variations in the structural parameters of the ASE system.

6.1.2 SISO Gain Margins

Upper and lower gain margins are defined for a stable closed loop ASE system. The upper gain margin indicates the lowest relative increase in the loop gain $G_{v,i,j}$ for which the closed loop system is unstable. Using the notation of Eq. (6.1), the upper gain margin is the smallest $g_{i,j} > 1$ that causes closed loop instability. Similarly, the lower gain margin indicates the lowest relative decrease in $G_{v,i,j}$, i.e., the largest $0 < g_{i,j} < 1$, that leads to an unstable closed loop system. According to the Nyquist stability criterion, gain margins are the reciprocals of the open loop transfer function gain, evaluated at the phase crossover frequencies defined as the frequencies for which the transfer function phase equals to 0° . The 0° (and not the classical -180°) phase crossing is used because of the positive feedback assumption in Eq. (4.30). Among all the phase crossover points, the two closest to $+1$ in the complex Nyquist plane determine the upper and lower gain margins.

In the ASE context, the SISO transfer function of interest is $T_{oc,j,i}(s)$ defined in Eq. (6.7). To compute the gain margins, it is necessary to determine the phase crossover frequencies ω_{pco} for which $T_{oc,j,i}(j\omega_{pco})$ is real and positive. For that, the matrices $[L]$ and $[N]$ are constructed as follows

$$[L] = \begin{bmatrix} [A_{oc}] & [0]_{n_v \times n_v} & \{b_{oc_i}\} \\ [0]_{n_v \times n_v} & -[A_{oc}]^T & -[c_{oc_j}]^T \\ [c_{oc_j}] & -\{b_{oc_i}\}^T & 0 \end{bmatrix} \quad [N] = \begin{bmatrix} [I]_{2n_v \times 2n_v} & 0 \\ 0 & \dots\dots\dots 0 \end{bmatrix} \quad (6.8)$$

where $n_v \times n_v$ is the dimension of $[A_{oc}]$. The phase crossover frequencies are the imaginary parts of the purely imaginary generalized eigenvalues of $[L]$ and $[N]$, i.e.

$$[L] \{x_k\} = \lambda_k [N] \{x_k\}, \quad k = 1, \dots, n_v \quad (6.9)$$

and $\{x_k\}$ are the corresponding generalized right eigenvectors. Among all the purely imaginary λ_k -s only the ones with real and positive $T_{oc,j,i}(\lambda_k)$ are relevant to finding upper and

lower gain margins, leading to the set

$$\bar{\omega} := \left\{ \text{Imag}(\lambda_k) \left| \begin{array}{l} \text{Real}(\lambda_k) = 0, \quad \text{Imag}(\lambda_k) > 0, \\ \text{Real}(T_{ocj,i}(\lambda_k)) > 0, \quad \text{Imag}(T_{ocj,i}(\lambda_k)) = 0 \end{array} \right. \right\} \quad (6.10)$$

By definition, the upper and lower gain margins are determined as

$$GM_u = \frac{1}{\underset{\bar{\omega}}{Max} \{0 < T_{ocj,i}(j\bar{\omega}) < 1\}} \quad (6.11)$$

$$GM_l = \frac{1}{\underset{\bar{\omega}}{Min} \{1 < T_{ocj,i}(j\bar{\omega})\}} \quad (6.12)$$

The expressions above yield the phase crossover frequencies, ω_{pco}^u and ω_{pco}^l , which correspond to the upper gain margin, GM_u , and lower gain margin, GM_l , respectively. Therefore,

$$GM_{u,l} = \frac{1}{T_{ocj,i}(j\omega)} \Big|_{\omega_{pco}^{u,l}} \quad (6.13)$$

and in decibels,

$$GM_{u,l}[\text{dB}] = 20 \log GM_{u,l} = -20 \log T_{ocj,i}(j\omega) \Big|_{\omega_{pco}^{u,l}} \quad (6.14)$$

Note: Some systems may have no upper and/or lower gain margins (often set to $\pm\infty$ [dB]). In these cases, the gain margins and their corresponding sensitivities, discussed below, are not calculated.

6.1.3 SISO Phase Margins

Upper and lower phase margins are defined for a stable closed loop ASE system. The upper phase margin indicates the lowest additional loop phase lag for which the closed loop system is unstable. Using the notation of Eq. (6.1), the upper phase margin is minus the largest $\phi_{i,j} < 0$ that causes closed loop instability. Similarly, the lower phase margin indicates the lowest additional loop phase lead, i.e., minus the smallest $\phi_{i,j} > 0$, that leads to an unstable closed loop system. Based on the Nyquist stability criterion for positive feedback systems,

phase margins are evaluated at the gain crossover frequencies (defined as the frequencies for which the transfer function gain is unity) and equal to the transfer function phase at these frequencies. Among all the gain crossover points, the two closest to +1 in the complex Nyquist plane are used to determine the upper and lower phase margins. By convention, the upper phase margin is positive and the lower phase margin is negative.

In the ASE context, $T_{ocj,i}(s)$ of Eq. (6.7) is used as the open loop transfer function for phase margin calculations. The gain crossover frequencies ω_{gco} are found by computing the eigenvalues of the Hamiltonian matrix $[H]$ defined by

$$[H] = \begin{bmatrix} [A_{oc}] + \{b_{oc,i}\} [c_{ocj}] \frac{d_{ocj,i}}{\bar{d}_{j,i}} & \{b_{oc,i}\} \{b_{oc,i}\}^T / \bar{d}_{j,i} \\ -[c_{ocj}]^T [c_{ocj}] / \bar{d}_{j,i} & -\left[[A_{oc}] + \{b_{oc,i}\} [c_j] \frac{d_{j,i}}{\bar{d}_{j,i}} \right]^T \end{bmatrix} \quad (6.15)$$

where $\bar{d}_{j,i} = 1 - d_{ocj,i}^2$. Among these eigenvalues λ_k , $i = k, \dots, 2n_v$, only purely imaginary ones for which $|T_{ocj,i}(\lambda_k)| = 1$ are used to determine the upper and lower phase margins, leading to the set

$$\bar{\omega} := \left\{ \text{Imag}(\lambda_k) \mid \text{Real}(\lambda_k) = 0, \text{Imag}(\lambda_k) > 0, |T_{ocj,i}(\lambda_k)| = 1 \right\} \quad (6.16)$$

The upper and lower phase margins are determined as

$$PM_u = \underset{\bar{\omega}}{\text{Min}} \left\{ 0^\circ \leq \angle T_{ocj,i}(j\bar{\omega}) \leq 180^\circ \right\} \quad (6.17)$$

$$PM_l = \underset{\bar{\omega}}{\text{Max}} \left\{ -180^\circ \leq \angle T_{ocj,i}(j\bar{\omega}) \leq 0^\circ \right\} \quad (6.18)$$

where $\angle T_{ocj,i}(j\bar{\omega})$ is manipulated to be in the range $-180^\circ \leq \angle T_{ocj,i}(j\bar{\omega}) \leq 180^\circ$. Note that the above expressions yield the conventionally assumed $PM_u > 0$ and $PM_l < 0$. These expressions also yield the gain crossover frequencies, ω_{gco}^u and ω_{gco}^l , which correspond to the upper phase margin, PM_u , and lower phase margin, PM_l , respectively. Therefore,

$$PM_{u,l} = \angle T_{ocj,i}(j\omega) \Big|_{\omega_{gco}^{u,l}} \quad (6.19)$$

or

$$PM_{u,l} = \tan^{-1} \left(\frac{\text{Imag}[T_{ocj,i}(j\omega)]}{\text{Real}[T_{ocj,i}(j\omega)]} \right) \bigg|_{\omega_{gc}^{u,l}} \quad (6.20)$$

Note: Some systems may have no upper and/or lower phase margins (often set to $\pm\infty[^\circ]$). In these cases, the phase margins and their corresponding sensitivities, discussed below, are not calculated.

6.1.4 Sensitivities of SISO Gain Margins

In this section the sensitivities of the upper and lower gain margins with respect to a design variable are derived. The gain margins are computed for the controller gain $G_{v,i,j}$ variations, while the design variables include structural variables and the controller variable gain matrix $[G_v]$ entries, all grouped in the vector $\{v\}$.

The sensitivity of the gain margins expressed in decibels are given by

$$\frac{\partial GM_{u,l}[\text{dB}]}{\partial v_i} = \frac{20/\ln 10}{GM_{u,l}} \frac{\partial GM_{u,l}}{\partial v_i} \quad (6.21)$$

where $\partial GM_{u,l}/\partial v_i$ is the regular (not in decibel) gain margin sensitivity.

The gain margin sensitivities with respect to $G_{v,i,j}$ are given simply by

$$\frac{\partial GM_{u,l}}{\partial G_{v,i,j}} = -\frac{GM_{u,l}}{\bar{G}_{v,i,j}} \quad (6.22)$$

or in decibels

$$\frac{\partial GM_{u,l}[\text{dB}]}{\partial G_{v,i,j}} = -\frac{20/\ln 10}{\bar{G}_{v,i,j}} \quad (6.23)$$

To compute the gain margin sensitivities with respect to the other design variables v_i , the matrix $[A_{GM_{u,l}}]$ is constructed

$$[A_{GM_{u,l}}] = \left[[A_{oc}] + \frac{GM_{u,l}}{1 - d_{ocj,i} GM_{u,l}} \{b_{oc_i}\} [c_{oc_j}] \right] \quad (6.24)$$

Note that $j\omega_{pco}^{u,l}$ is an eigenvalue of $[A_{GM_{u,l}}]$. The gain margin sensitivities are given by

$$\frac{\partial GM_{u,l}}{\partial v_i} = - \frac{\text{Real} \left(\frac{\{Y\}^T \frac{\partial A_{GM_{u,l}}}{\partial v_i} \{X\}}{\{Y\}^T \{X\}} \right)}{\text{Real} \left(\frac{\{Y\}^T \frac{\partial A_{GM_{u,l}}}{\partial GM_{u,l}} \{X\}}{\{Y\}^T \{X\}} \right)} \quad (6.25)$$

where $\{X\}$ and $\{Y\}^T$ are right and left eigenvectors of $[A_{GM_{u,l}}]$ given by

$$[A_{GM_{u,l}}] \{X\} = j\omega_{pco}^{u,l} \{X\} \quad (6.26)$$

$$\{Y\}^T [A_{GM_{u,l}}] = j\omega_{pco}^{u,l} \{Y\}^T \quad (6.27)$$

and

$$\frac{\partial A_{GM_{u,l}}}{\partial GM_{u,l}} = \frac{1}{(1 - d_{ocj,i} GM_{u,l})^2} \{b_{oc_i}\} [c_{oc_j}] \quad (6.28)$$

The sensitivity $\partial A_{GM_{u,l}} / \partial v_i$ is constructed using the results of Section 4.5.

6.1.5 Sensitivities of SISO Phase Margins

Upper and lower phase margin sensitivities are computed with respect to the design variable vector $\{v\}$ defined in the previous section. To compute these sensitivities, the matrix $[A_{PM_{u,l}}]$ is constructed

$$[A_{PM_{u,l}}] = \left[[A_{oc}] + \frac{1}{e^{jPM_{u,l}[\text{rad}]} - d_{ocj,i}} \{b_{oc_i}\} [c_{oc_j}] \right] \quad (6.29)$$

where $PM_{u,l}[\text{rad}]$ is the phase margin expressed in radians. Note that $[A_{PM_{u,l}}]$ is complex and $j\omega_{pco}^{u,l}$ is its eigenvalue.

The phase margin sensitivities are given by

$$\frac{\partial PM_{u,l}}{\partial v_i} = - \frac{\text{Real} \left(\frac{\{Y\}^T \frac{\partial A_{PM_{u,l}}}{\partial v_i} \{X\}}{\{Y\}^T \{X\}} \right)}{\text{Real} \left(\frac{\{Y\}^T \frac{\partial A_{PM_{u,l}}}{\partial PM_{u,l}[\text{rad}]} \{X\}}{\{Y\}^T \{X\}} \right)} \cdot \frac{180}{\pi} \quad (6.30)$$

where $\{X\}$ and $\{Y\}^T$ are right and left eigenvectors of $[A_{PM_{u,l}}]$ given by

$$[A_{PM_{u,l}}] \{X\} = j\omega_{gco}^{u,l} \{X\} \quad (6.31)$$

$$\{Y\}^T [A_{PM_{u,l}}] = j\omega_{gco}^{u,l} \{Y\}^T \quad (6.32)$$

and

$$\frac{\partial A_{PM_{u,l}}}{\partial PM_{u,l}[\text{rad}]} = - \frac{j e^{jPM_{u,l}[\text{rad}]}}{(e^{jPM_{u,l}[\text{rad}]} - d_{ocj,i})^2} \{b_{oc_i}\} [c_{oc_j}] \quad (6.33)$$

Again, the sensitivity $\partial A_{PM_{u,l}}/\partial v_i$ is constructed using the results of Section 4.5.

6.2 MIMO Stability Margins and Sensitivities

Following Ref. 14, the MIMO stability margins are defined by introducing ASE system uncertainties at the plant input or output as described in Figure 6.2.

The input and output MIMO stability margins are defined with respect to uncertainties (variations) in the matrices $[L_i]$ and $[L_o]$, which are assumed to be diagonal, i.e.

$$[L_i] = \text{diag} [g_l^i e^{j\phi_l^i}], \quad l = 1, 2, \dots, N_i \quad (6.34)$$

$$[L_o] = \text{diag} [g_k^o e^{j\phi_k^o}], \quad k = 1, 2, \dots, N_o \quad (6.35)$$

where N_i and N_o are the number of inputs and outputs, respectively, to the ASE model.

At the nominal condition, $g_l^i = g_k^o = 1$ and $\phi_l^i = \phi_k^o = 0 \quad \forall l, k$, i.e., $[L_i] = I_{N_i \times N_i}$ and

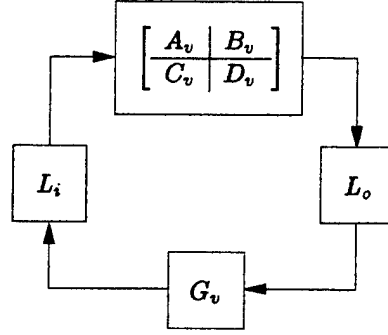


Figure 6.2: MIMO stability margin evaluation setup.

$[L_o] = I_{N_o \times N_o}$. Sufficient conditions for a guaranteed gain margin \bar{g}^i and phase margin $\bar{\phi}^i$ at *any* input to the gain-open ASE plant are

$$\left[(1 - 1/\bar{g}^i)^2 + 2(1 - \cos \bar{\phi}^i)/\bar{g}^i \right]^{1/2} < \underline{\sigma} \{I - G_v P_v\} \quad (6.36)$$

or

$$\left[(1 - \bar{g}^i)^2 + 2\bar{g}^i(1 - \cos \bar{\phi}^i) \right]^{1/2} < \underline{\sigma} \{I - [G_v P_v]^{-1}\} \quad (6.37)$$

where

$$[P_v(s)] = [C_v][sI - A_v]^{-1}[B_v] + [D_v]$$

and $\underline{\sigma}\{\cdot\}$ is the minimum singular value of the argument matrix evaluated at $s = j\omega \forall \omega \geq 0$. Sufficient conditions for output gain and phase margins are similar to the inequalities of Eqs. (6.36) and (6.37) except of replacing the $[G_v P_v]$ terms with $[P_v G_v]$.

The inequalities of Eqs. (6.36) and (6.37) on the ASE system minimum singular values can serve as MIMO stability margins in the multidisciplinary optimization process. Their sensitivities with respect to a design parameter p are computed analytically from the singular value derivative expression

$$\frac{\partial \underline{\sigma}\{H\}}{\partial p} = \text{Real} \left(\underline{u}^* \frac{\partial H}{\partial p} \underline{v} \right) \quad (6.38)$$

where \underline{u} and \underline{v} are, respectively, the right and left normalized singular vectors of the matrix $[H]$, corresponding to the minimum singular value $\underline{\sigma}\{H\}$. In the ASE MIMO case,

$$[H] = [I] - [G_v] \left[[C_v][sI - A_v]^{-1}[B_v] + [D_v] \right] \quad (6.39)$$

and the evaluation of the derivative $\partial \underline{\sigma}\{H\} / \partial p$ facilitates the sensitivities of $[A_v]$, $[B_v]$, $[C_v]$ and $[D_v]$ which were discussed earlier in the SISO margin section.

Chapter 7

Continuous Gust Response

The time-domain ASE model for continuous gust response analysis is based on the ASE model of Chapter 4, augmented by gust states and excited by a gust velocity input. The formulation is based on the gust modeling of Ref. 5. It assumes a single gust pattern, either vertical or lateral, represented by the spectral properties of the gust velocity amplitude. The gusts are assumed to be spanwise uniform. Kinematic load modes and the associated aerodynamic and inertial coefficient matrices facilitate the use of section loads as design constraints.

7.1 Equation of Motion

The second-order time-domain equation of motion of the structure was defined in Eq. (2.23), with the generalized external forces represented by $\{P_h(t)\}$. The external forces for stability analysis were expressed in Section 4, where they included aerodynamic forces due to structural dynamics, and inertial and aerodynamic forces due to control-surface motion. These loads can be considered as part of the internal dynamics of the closed-loop aeroservoelastic system. Gust response analysis requires the addition of gust input loads. When output section loads are required, generalized aerodynamic loads associated with kinematic load modes are required as well.

The generalized aerodynamic forces are defined in the frequency domain in Eq. (2.38). The aerodynamic force coefficient (AFC) matrices, including the gust column $\{Q_{hG}\}$, are first calculated at several user-defined tabulated reduced frequency values, k_t . The tabulated matrices are used for approximating the AFC matrix as a rational function of k in the entire frequency domain, as described in Chapter 3. An expansion to the entire Laplace domain is performed by replacing ik in the rational expression by the non-dimensional Laplace variable $p = sb/V$, which yields Eq. (3.2). The substitution of $p = sb/V$ in the expression for $[\tilde{Q}_h(p)]$ of Eq. (3.2), and the subsequent construction of the state-space equations for stability analysis were discussed in Chapter 4. The expanded version of Eq. (4.1), which includes the gust related coefficients, reads

$$\begin{bmatrix} \tilde{Q}_h(s) \\ \tilde{Q}_L(s) \end{bmatrix} = \begin{bmatrix} A_{h0} \\ A_{L0} \end{bmatrix} + \frac{b}{V} \begin{bmatrix} A_{h1} \\ A_{L1} \end{bmatrix} s + \frac{b^2}{V^2} \begin{bmatrix} A_{h2} \\ A_{L2} \end{bmatrix} s^2 + \begin{bmatrix} D_h \\ D_L \end{bmatrix} \left([I]s - \frac{V}{b}[R] \right)^{-1} [E]p \quad (7.1)$$

where the coefficient matrices are column partitioned as

$$\begin{bmatrix} A_{hn} \\ A_{Ln} \end{bmatrix} = \begin{bmatrix} A_{hhn} & A_{hcn} & A_{hGn} \\ A_{Lhn} & A_{Lcn} & A_{LGn} \end{bmatrix} \quad (n = 0, 1, 2), \quad [E] = [E_h \quad E_c \quad E_G]$$

When the design values are different than the ones for which the approximation matrices were calculated, $\{A_{hGn}\}$ is updated by Pre-multiplying its baseline value by $[\psi]^T$, and $[A_{Lhn}]$ is updated by post-multiplying it by $[\psi]$, similarly to the other matrix updated in Eq. (4.2).

To avoid coefficients associated with the second time derivative of the gust velocity. Approximation constraints should be applied to the gust columns to yield $\{A_{hG_2}\} = 0$ and $\{A_{LG_2}\} = 0$. As discussed in Chapter 3, the approximation matrices $[A_{hn}]$, $[D_h]$ and $[E]$ are solved for while ignoring the section-loads data. The $[A_{Ln}]$ and $[D_L]$ matrices are then solved for with a fixed $[E]$.

The augmenting aerodynamic state vector is defined here by its Laplace transform as

$$\{x_a(s)\} = \left([I]s - \frac{V}{b}[R] \right)^{-1} \left([E_h]\{\xi(s)\} + [E_c]\{\delta_c(s)\} + \frac{1}{V}\{E_G\}w_G(s) \right) s \quad (7.2)$$

Equations (3.1), (7.1) and (7.2) add a gust related term to the generalized aerodynamic force vector $\{P_h^a(s)\}$ of Eq. (4.4),

$$\{P_h^a(s)\}_G = -\frac{q}{V} \left(\{A_{hG_0}\} + \frac{b}{V} \{A_{hG_1}\} s \right) w_G(s) \quad (7.3)$$

Equations (2.23), (2.28), (4.4) and (7.3) yield the state-space aeroelastic equation of motion for open-loop response analysis

$$\{\dot{x}_{ae}\} = [A_{ae}]\{x_{ae}\} + [B_{ae}]\{u_{ae}\} + [B_{aw}]\{\tilde{w}_G\} \quad (7.4)$$

where $\{x_{ae}\}$, $\{u_{ae}\}$, $[A_{ae}]$ and $[B_{ae}]$ are defined in Eq. (4.5) and

$$\{\tilde{w}_G\} = \begin{Bmatrix} w_G \\ \dot{w}_G \end{Bmatrix} \quad [B_{aw}] = \begin{bmatrix} 0 & 0 \\ -\frac{q}{V}[\bar{M}]^{-1}\{A_{hG_0}\} & -\frac{qb}{V^2}[\bar{M}]^{-1}\{A_{hG_1}\} \\ 0 & \frac{1}{V}\{E_G\} \end{bmatrix}$$

where $[\bar{M}]$ defined in Eq. (4.5).

Sensor readings of the aeroelastic plant were defined in Eqs. (4.6) to (4.9). The only effects of the gust inputs on sensor readings are in the case of acceleration output, where the expression for y_a in Eq. (4.8) is supplemented by

$$y_{aG} = [C_{aG}]\{\tilde{w}_G\} \quad (7.5)$$

where

$$[C_{aG}] = -[\phi_y][\bar{M}]^{-1} \begin{bmatrix} \frac{q}{V}\{A_{hG_0}\} & \frac{qb}{V^2}\{A_{hG_1}\} \end{bmatrix}$$

which expands Eq. (4.9) to become

$$\{y_{ae}\} = [C_{ae}]\{x_{ae}\} + [D_{ae}]\{u_{ae}\} + [C_{Ga}]\{\tilde{w}_G\} \quad (7.6)$$

where the only non-zero rows in $[C_{Ga}]$ are those associated with acceleration signals, which are taken from $[C_{aG}]$ of Eq. (7.5).

The plant equations of motion, Eqs. (4.14) and (4.15), become

$$\begin{aligned}\{\dot{x}_p\} &= [A_p]\{x_p\} + [B_p]\{u_p\} + [B_{pw}]\{\tilde{w}_G\} \\ \{y_p\} &= [C_p]\{x_p\} + [C_{Ga}]\{\tilde{w}_G\}\end{aligned}\quad (7.7)$$

where

$$[B_{pw}] = \begin{bmatrix} B_{aw} \\ 0 \end{bmatrix}$$

The vehicle equations of motion, Eq. (4.28) become

$$\begin{aligned}\{\dot{x}_v\} &= [A_v]\{x_v\} + [B_v]\{u_v\} + [B_{vw}]\{\tilde{w}_G\} \\ \{y_v\} &= [C_v]\{x_v\} + [D_v]\{u_v\} + [C_{Gv}]\{\tilde{w}_G\}\end{aligned}\quad (7.8)$$

where

$$[B_{vw}] = \begin{bmatrix} B_{pw} \\ B_{c_2} I_{cp} C_{G_2} \end{bmatrix}, \quad [C_{Gv}] = \begin{bmatrix} C_{Ga} \\ D_{c_{12}} I_{cp} C_{G_2} \end{bmatrix}$$

The equation of motion of the closed-loop aeroservoelastic system is

$$\{\dot{x}_v\} = [\bar{A}_v]\{x_v\} + [\bar{B}_{vw}]\{\tilde{w}_G\} \quad (7.9)$$

where $[\bar{A}_v]$ is the closed-loop system matrix defined in Eq. (4.33) and

$$[\bar{B}_{vw}] = [B_{vw}] + [B_v][G_v][I - D_v G_v]^{-1} [C_{G_v}]$$

Output parameters $\{y_R\}$ which are of interest for dynamic response analysis are expressed in terms of the plant states, similarly to the sensor readings of Eq. (7.7),

$$\{y_R\} = [C_{pR}]\{x_p\} + [C_{GaR}]\{\tilde{w}_G\} \quad (7.10)$$

where, similarly to $[C_{Ga}]$, $[C_{GpR}] = 0$ except for acceleration response rows.

7.2 Gust Model

The description of the gust mode and the way gust column in the generalized aerodynamic matrix is calculated, are given in the theoretical manual of the ZAERO module. We deal

in this section with the statistical properties of the gust velocity and their realization in state-space modeling.

It is assumed that the gusts are generated in a stationary, Gaussian, stationary random process. A continuous atmospheric is defined by its root-mean-square (RMS) value and power spectral density (PSD) function. RMS gust values, σ_{w_G} , for aircraft design are defined by aviation regulations. A classical formula for the gust PSD is that of Dryden,

$$\Phi_{w_G}(\omega) = \sigma_{w_G}^2 \tau_g \frac{1 + 3(\omega\tau_g)^2}{[1 + (\omega\tau_g)^2]^2} \quad (7.11)$$

where $\tau_g = L_g/V$ where L_g is the scale of turbulence typically 2500 ft for aircraft design. This formula is consistent with the relation between RMS value and PSD function in the theory of stochastic processes,

$$\sigma_{w_G}^2 = \frac{1}{2\pi} \int_{-\infty}^{\infty} \Phi_{w_G}(\omega) d\omega = \frac{1}{\pi} \int_0^{\infty} \Phi_{w_G}(\omega) d\omega \quad (7.12)$$

The expression of Dryden appears some time with a π in the denominator, which agrees with the formula traditionally used by aeroelasticians,

$$\sigma_{w_G}^2 = \int_0^{\infty} \Phi_{w_G}(\omega) d\omega \quad (7.13)$$

A more modern PSD formula, but somewhat more complicated, is that of Von Karman,

$$\Phi_{w_G}(\omega) = \sigma_{w_G}^2 \tau_g \frac{1 + \frac{8}{3}(1.339\omega\tau_g)^2}{[1 + (1.339\omega\tau_g)^2]^{11/6}} \quad (7.14)$$

To facilitate the use of modern algebraic tools for calculating the structural response to continuous gust excitation, we want to describe the gust-response process by a state-space model excited by white noise. For this purpose we need to define a gust filter that, when excited by white noise, produces the gust PSD function. The transfer function of a filter that produces Dryden's formula is

$$T_g(s) \equiv \frac{w_G(s)}{w(s)} = \sigma_{w_G} \frac{\sqrt{3}\tau_g^{-1/2}s + \tau_g^{-3/2}}{(s + \frac{1}{\tau_g})^2} \quad (7.15)$$

where w is a white-noise parameter with $\Phi_w = 1$. A state-space realization of this filter would result with direct white-noise excitation of the aircraft dynamics, and hence non-converged RMS acceleration response. To avoid that, we add a low-pass filter which modifies $T_g(s)$ to be

$$\tilde{T}_g(s) = \frac{a}{s+a} T_g(s) \quad (7.16)$$

A state-space realization of $\tilde{T}_g(s)$ is

$$\begin{aligned} \{\dot{x}_g\} &= [A_g]\{x_g\} + \{B_g\}w \\ \{\tilde{w}_G\} &= [C_g]\{x_g\} \end{aligned} \quad (7.17)$$

where

$$\begin{aligned} [A_g] &= \begin{bmatrix} 0 & 1 & 0 \\ -\tau_g^{-2} & -2/\tau_g & a \\ 0 & 0 & -a \end{bmatrix} & \{B_g\} &= \begin{Bmatrix} 0 \\ 0 \\ \sigma_{w_G} \end{Bmatrix} \\ [C_g] &= \begin{bmatrix} \tau_g^{-3/2} & \sqrt{3}\tau_g^{-1/2} & 0 \\ -\sqrt{3}\tau_g^{-5/2} & (1-2\sqrt{3})\tau_g^{-3/2} & \sqrt{3}a\tau_g^{-1/2} \end{bmatrix} \end{aligned}$$

Since Von Karman's PSD, Eq. (7.14), is a non-rational function of ω , it can not be modeled exactly by a transfer function. Reference 16 suggested the 3rd order filter

$$T_g = \sigma_{w_G} \sqrt{\tau_g} \frac{(1 + 2.618\tau_g s)(1 + 0.1298\tau_g s)}{(1 + 2.083\tau_g s)(1 + 0.823\tau_g s)(1 + 0.0898\tau_g s)} \quad (7.18)$$

which yields good fit in the range $0 \leq \tau_g \omega \leq 20$. Hoblit¹⁷ suggested

$$\begin{aligned} T_g &= \sigma_{w_G} \sqrt{\tau_g} \times \\ &\frac{(1 + 2.187\tau_g s)(1 + 0.1833\tau_g s)(1 + 0.021\tau_g s)}{(1 + 1.339\tau_g s)(1 + 1.118\tau_g s)(1 + 0.1277\tau_g s)(1 + 0.0146\tau_g s)} \end{aligned} \quad (7.19)$$

which is good for $0 \leq \tau_g \omega \leq 200$. Both approximations of Von Karman's PSD function require additional low-pass filter to yield a state-space realization without an output noise term, as in Eq. (7.17). With the low-pass filter, Eq. (7.18) yields a 4-state filter, and Eq. (7.19) yields a 5-state one.

7.3 Gust Response Analysis

Augmentation of the aeroservoelastic equation (7.9) by the gust filter, Eq. (7.17), yields

$$\{\dot{x}_1\} = [A_1]\{x\} + \{B_{1w}\}w \quad (7.20)$$

where

$$\{x_1\} = \begin{Bmatrix} x_v \\ x_g \end{Bmatrix} \quad [A_1] = \begin{bmatrix} [\bar{A}_v] & [B_{vw}][C_g] \\ 0 & [A_g] \end{bmatrix} \quad \{B_{1w}\} = \begin{Bmatrix} 0 \\ B_g \end{Bmatrix}$$

Gust response parameters expressed by Eq. (7.10) become

$$\{y_1\} = [C_1]\{x_1\} \quad (7.21)$$

where

$$[C_1] = \begin{bmatrix} [C_{pR}] & [C_{GaR}][C_g] \end{bmatrix}$$

The response parameters include discrete structural response and integrated section loads. The discrete parameters are displacements, velocities and accelerations that were formulated in Eqs. (4.6) to (4.8) and (7.5). Section loads can also be expressed in the form of Eq. (7.21). Equations (2.40, 7.1, 7.2, 7.17) yield the time-domain aerodynamic loads

$$\begin{aligned} \{P_L^a\} = & \\ & - q \begin{bmatrix} A_{Lh_0} & \frac{b}{V} A_{Lh_1} & D_L & A_{Lc_0} & \frac{b}{V} A_{Lc_1} & \frac{b^2}{V^2} A_{Lc_2} & 0 & \frac{1}{V} A_{LG_0} C_g & \frac{b}{V^2} A_{LG_1} C_g \end{bmatrix} \{x_1\} \\ & - q \frac{b^2}{V^2} [A_{Lh_2}] \{\ddot{\xi}\} \end{aligned} \quad (7.22)$$

where $\{\ddot{\xi}\}$ can be expressed in terms of $\{x_1\}$ by using the associated row partition in Eq.(7.20).

Rigid-body displacement modes with no aerodynamic stiffness (in X , Y , Z and θ_x) cause zero roots. The rows and columns associated with the deflection states of these modes should be removed to avoid singularity in the solution of the Lyapunov equations given below. We

assume now that the first state in $\{x_1\}$ after this removal are θ_y in the symmetric case and θ_z in the anti-symmetric case. Other rigid-body motion modes that have a zero eigenvalue are the symmetric one with $\theta_y = \dot{Z}/V$ and the antisymmetric $\theta_z = -\dot{Y}/V$. Such singularity is eliminated by calculating the associated eigenvector, creating a transformation matrix $[T]$ in which the first column of a unit matrix is replaced by the eigenvector, and performing the transformation

$$\{x_2\} = [T]^{-1}\{x_1\} \quad (7.23)$$

which yields

$$\begin{aligned} \{\dot{x}\} &= [A]\{x\} + \{B_w\}w \\ \{y\} &= [C]\{x\} \end{aligned} \quad (7.24)$$

where $\{x\}$ is $\{x_2\}$ with the first term truncated, $[A]$ is $[A_2] = [T]^{-1}[A_1][T]$ with the first row and the first column truncated, $[B_w]$ is $[B_{2w}] = [T][B_{1w}]$ with the first row truncated, and $[C]$ is $[C_2] = [C_1][T]$ with the first column truncated.

A state covariance matrix $[X]$ is defined by the expected value

$$[X] = E[\{x\}\{x\}^T] \quad (7.25)$$

When w of Eq. (7.20) represents a unit-intensity white-noise process, $[X]$ satisfies the Lyapunov equation

$$[A][X] + [X][A]^T = -\{B_w\}\{B_w\}^T \quad (7.26)$$

Efficient solution is obtained via Schur decomposition $[A] = [U][T][U]^T$ where $[U]$ is a unitary matrix, $[U][U]^T = [I]$, and $[T]$ is an upper triangular matrix. A unique solution for $[X]$ is obtained when $[A]$ has no roots with real part equals zero. The output covariance matrix is related to $[X]$ by

$$[Y] = E[\{y\}\{y\}^T] = E[[C]\{x\}\{x\}^T[C]^T] = [C][X][C]^T \quad (7.27)$$

The diagonal of $[Y]$ contains the mean-square output response

$$\sigma_y^2 = [C_y][X][C_y]^T \quad (7.28)$$

where $[C_y]$ is a row in $[C]$ of Eq. (7.24)

7.4 Sensitivity Analysis

The derivatives of gust response parameters with respect to the design variables are based on the sensitivity of the $[A_1]$ and $[C_1]$ in Eq. (7.20) and (7.21). These are transformed to the derivatives of $[A]$ and $[C]$ in the same way $[A_1]$ and $[C_1]$ are transformed into $[A]$ and $[C]$ in Section 7.5. The derivatives of $[A_1]$ are based on the derivatives of $[\bar{A}]$ discussed in Section 4.5, the derivatives of $[B_{vw}]$ which are non zero only with acceleration sensors. The derivatives of $[A_g]$ and $[C_g]$ and $\{B_{1w}\}$ are zero. The derivatives of $[C_1]$ are non zero only when accelerations are involved, which happens in acceleration and section-loads responses.

The differentiation of Eq. (7.28) with respect to a design variable v_i yields

$$\frac{\partial}{\partial v_i} \sigma_y^2 = [C_y] \frac{\partial}{\partial v_i} [X] [C_y]^T + 2 \frac{\partial}{\partial v_i} [C_y] [X] [C_y]^T \quad (7.29)$$

The derivatives of $[X]$ are obtained from the differentiation of Eq. (7.26), which yields the Lyapunov equation

$$[A] \frac{\partial}{\partial v_i} [X] + \frac{\partial}{\partial v_i} [X] [A]^T = - \frac{\partial}{\partial v_i} [A] [X] - [X] \frac{\partial}{\partial v_i} [A]^T \quad (7.30)$$

which is solved for $\partial[X]/\partial v_i$, which is then substituted in Eq. (7.26) for the derivatives of the mean-square responses. The Schur decomposition of $[A]$ can be used for all responses and their sensitivity derivatives.

References

1. Roger, K.L., "Airplane Math Modeling and Active Aeroelastic Control Design", **AGARD-CP-228**, 1977, pp. 4.1-4.11.
2. Karpel, M. "Design for Active and Passive Flutter Suppression and Gust Alleviation", **NASA CR-3482**, 1981.
3. Karpel, M., "Design for Active Flutter Suppression and Gust Alleviation Using State-Space Aeroelastic Modeling", *Journal of Aircraft*, Vol. 19, No. 3, 1982, pp. 221-227.
4. Karpel, M., "Time-Domain Aeroservoelastic Modeling Using Weighted Unsteady Aerodynamic Forces", *Journal of Guidance, Control, and Dynamics*, Vol.13, No. 1 , pp. 30-37, 1990.
5. Karpel, M., "Extension to the Minimum-State Aeroelastic Modeling Method", *AIAA Journal*, Vol. 29, No. 11, 1991, pp. 2007-2009.
6. Karpel, M. and Hoadley, S.T., "Physically Weighted Approximations of Unsteady Aerodynamic Forces Using the Minimum-State Method", **NASA TP-3025**, 1991.
7. Karpel, M., "Size-Reduction Techniques for the Determination of Efficient Aeroservoelastic Models", Academic Press, *Advances in Control and Dynamic Systems*, Vol. 54, 1992, pp. 263-295.

8. Karpel, M. and Strul, E., "Minimum-State Unsteady Aerodynamic Approximations with Flexible Constraints", *J. Aircraft*, Vol. 33, No. 6, 1996, pp. 1190-1196.
9. Neill, D.J., Herendeen, D.L. and Venkayya, V.B., "ASTROS Enhancements, Volume III - Theoretical Manual", WL-TR-3006, May 1995.
10. Karpel, M. and Presente, E., "Structural Dynamic Loads in Response to Impulsive Excitation", *Journal of Aircraft*, Vol. 32, No. 4, 1995, pp. 853-861.
11. Hoadley, S.T. and Karpel, M., "Application of Aeroservoelastic Modeling Using Minimum-State Unsteady Aerodynamic Approximations", *Journal of Guidance, Control and Dynamics*, Vol. 14, No. 6, 1991, pp. 1267-1276.
12. Karpel, M., "Sensitivity Derivatives of Flutter Characteristics and Stability Margins for Aeroservoelastic Design", *Journal of Aircraft*, Vol. 27 No. 4, 1990, pp. 368-375.
13. Karpel, M. and Wieseman, C. D., "Modal Coordinates for Aeroelastic Analysis with Large Local Structural Variations", *Journal of Aircraft*, Vol. 31, No. 2, 1994, pp. 396-403.
14. Mukhopadhyay, V., "Control Law Synthesis and Stability Robustness Improvement Using Constrained Optimization Techniques", *Control and Dynamic Systems*, Vol. 32, Academic Press, 1990, pp. 163-205.
15. Zole, A. and Karpel, M., "Continuous Gust Response and Sensitivity Derivatives Using State-Space Models", *Journal of Aircraft*, Vol. 31, No. 5, 1994, pp. 1212-1214.
16. Pototzki, A.S., Zeiler, T.A. and Perry, B., "Calculating Time-Correlated Gust Loads Using Matched Filter and Random Process Theories", *Journal of Aircraft*, Vol.28, No. 5, 1991, pp.346-352.

17. Hoblit, F.M., "Gust Loads on Aircraft: Concepts and Applications" AIAA Education Series, Washington, D.C., 1988.